YTUP

Journal of Thermal Engineering
https://jten.yildiz.edu.tr/
https://doi.org/10.47481/jten.0030

RESEARCH ARTICLE

Effect of modifications of auxiliary surface attached to a rectangular vortex generator

Subhankar Saha[1], Koushik Das[2,*]

[1]Department of Mechanical Engineering, National Institute of Technology Meghalaya, Sohra, Meghalaya, 793108, India
[2]Department of Mechanical Engineering, National Institute of Technology Meghalaya, Sohra, Meghalaya, 793108, India

Abstract

Effective surface cooling techniques are in demand by various industries. Such techniques improve system performance and keep it within the safe thermal threshold. Thus, active heat dissipation methods are of utmost importance. One such method involves the use of an extended surface. Extended surfaces, like fin, improve the heat transfer rates by increasing the active heat dissipation area. On the other hand, a vortex generator enhances thermal dissipation by promoting boundary-layer interactions. Such interactions are strengthened by improving the developed differential pressure along the flow direction. An effective design of the extended surface helps in this process. Despite significant efforts in the past, earlier designs of vortex generators have shown limitations. This work presents a novel approach where the incorporation of a trapezoidal-shaped auxiliary surface, AP, onto a rectangular vortex generator, RVG, is proposed. A thorough parametric investigation is conducted using ANSYS Fluent to study various aspects of the AP, within a modified RVG. It includes a thorough study of its interior angles, width, height, and inclination angle with the principal part. The conservation equations are solved numerically. The proposed design yields improved performance. Configuring the interior angles of the AP at 120° increases the convective heat transfer coefficient by 11.13%. The modification also enhances the thermal performance factor by 9.9%. However, this enhancement is accompanied by a 3.53% rise in frictional losses. Further, a width of 0.01 m of the AP produces increments of 27.16% and 22.4% in the convective heat transfer coefficient and the thermal performance factor, respectively, as compared to the RVG. The corresponding frictional losses show an increase of 11.98%. Introducing the AP at the top of the principal part of the modified RVG results in a 27.16% increase in the Nusselt number. Moreover, varying the inclination angle of the AP produces a maximum increase of 27.64% in the Nusselt number and a 22.4% enhancement in the thermal performance factor.

Keywords: Thermal performance factor, vortex generator, conjugate heat transfer, primary vortex, auxiliary surface

Cite this article as: Saha, S., & Das, K. (2026). Effect of modifications of auxiliary surface attached to a rectangular vortex generator. Journal of Thermal Engineering, 12(4), 1282–1309. https://doi.org/10.47481/jten.0030

1. Introduction

In the modern world, every technological development demand sustainability. Reduction of system size and optimization of its energy consumption are two major factors toward such goals. However, in most industries, it is observed that power consumption increases along with the demand for smaller and lighter systems. Therefore, the miniaturization of systems with improved efficiency is the need of the hour. Higher energy consumption demands an effective heat dissipation system to avoid any thermal failure. Fins and vortex generators (VGs) are two popular components of such heat dissipation systems. Implementation of fins augments surface area and subsequently improves heat transfer. The use of VGs generates various helical fluid motions to enhance the convective thermal performance. This method is particularly effective and thus requires serious consideration.

The effectiveness of using VGs to improve heat transfer is reliant on various factors, including geometrical shapes [1-4]. Samadifar and Toghraie [5] studied the impact of different VGs, viz., RVG, wavy VG, etc. The investigation has been carried out numerically using the finite volume method (FVM), on a fin-plate heat exchanger with a triangular channel cross-section. The results show that the RVG improves the thermal performance of the system by 7%. However, the presence of VG in the system results in a higher-pressure drop. A 45° angle of attack (φ) is found to provide the best performance, with height

*Corresponding Author
E-mail Adress: koushik.das@nitm.ac.in

Submitted: 15 March 2024 ; **Accepted:** 12 June 2024

This paper was recommended for publication in revised form by Editor-in-Chief Ahmet Selim Dalkılıç

of the VG contributing to the thermal enhancement. Qian et al. [6] studied the heat exchangers with rectangle winglet VGs. The study found that the rectangle winglet helped in strengthening the weak areas of flow at the rear side of the tubes. This improves the thermal performance and resistance characteristics of the system. Biswas and Chattopadhyay [7] numerically studied the delta wing VGs in a rectangular channel. The Navier–Stokes equations and the energy equation were used to analyze thermal exchange between the fluid and the channel wall. The impacts of pierced holes, and Reynolds number (Re) were investigated. The average Nusselt number (Nu) is found to increase by a maximum of 34%. It was further reported that the improvement in thermal performance occurs at $\varphi = 26^{o}$.

Numerous works reported the application of VGs in heat exchangers with improved thermal performance. Different shapes of VGs have been tested using both numerical and experimental studies. The results indicate improved thermal behavior and better thermo-hydraulic performance. In addition, the placement and the orientation of the VGs are found to affect performance further. Luo et al. [8] focused on a new combination of a wavy fin and VG for heat exchangers to increase thermo-hydraulic performance. The findings indicate that the combination of VGs with wavy fins resulted in an increase in Nu by up to 33%. The thermal performance factor is also improved by a maximum of 26.4%. The study investigated different flow regimes and the impact of corrugation angles along with φ. In the laminar flow regime, the configuration with $\varphi = 45^{o}$ provides the best thermal performance. Sarangi and Mishra [9], in a separate study, evaluated the thermal behavior of rectangular winglet pairs (RWP). Positioning RWPs in a common-flow-up configuration enhances the heat transfer rate near the central tube. Thermal performance improves with φ up to 20^{o}, which resulted in a 60% increase in Nu. The winglets are found to perform better, when placed at 3.201 mm upstream in the streamwise direction and 7.2 mm spanwise. However, increased winglet numbers and upstream placement result in higher pressure drops. Thermal performance increased by 12%, 37% and 47%, with one, two and three winglet pairs, respectively.

Modi and Rathod [10] studied different rectangular winglet VGs (RWVGs) in heat exchangers, with different Re, varying between 400 and 1000. Compared to a reference case without VGs, RWVGs (wavy-up, wavy-down, curved-up, curved-up, curved-down) show an enhancement of heat transfer. Results show that the wavy-up setup provided the highest Nu. This indicates an increased thermal performance. However, curved-down RWVGs show a better balance in terms of thermo-hydraulic performance. In a separate study, Fiebig et al. [11] investigated wing-type VGs in heat exchangers for Re = 600-2700. Delta winglets were used in both inline and staggered tube systems. In the case of inline systems, VGs enhance thermal performance by up to 65%. However, these devices also increase the friction factor (f) by up to 45%. In the staggered setup, the thermal performance is found to increase by 9%. Gholami et al. [12] studied wavy rectangular winglets for a potential increment in thermal exchange. The Re varied between 400 and 800, with the φ as 30^{o}. The results show that the wavy rectangular winglet improves the thermal performance over the traditional VGs. The wavy-up setup improves thermal exchange better, with additional flow losses. Pressure drop is noticed with the wavy-down setup. In a different study, Sharma et al. [13] investigated a single triangular shaped winglet VG in a heat exchanger. The authors used triangular structures as auxiliary fins. The VGs were placed on the top and bottom parts of the system under a laminar flow condition. The results show that adding thickness, along with tilting of the VG at 45^{o}, enhances heat transfer by 19.7%. However, it also increases the pressure loss by 7.8%. This VG configuration reduces the size of the heat exchanger by almost 50%. Gonul and Okbaz [14] conducted a study on how VGs impact thermal performance. Different VG configurations were tested to enhance the flow structure and heat transfer efficiency. Higher vortex intensity and longer VGs are found to affect heat transfer. The expansion of secondary flow regions in the microchannel with an increasing number of VG pairs was also studied [14]. A maximum heat transfer enhancement of 230% was observed, with an increment in pressure loss of 950%. The maximum thermo-hydraulic performance factor was obtained at around 1.38. Välikangas et al. [15] studied delta winglet VGs for a possible enhancement in thermal characteristics. The study reported that the presence of VGs helps in forming longitudinal vortices and improves thermal exchange. It also shows reduced flow losses. The improved design yields a 5.23% improvement in overall performance as compared to the plain fin.

Researchers today emphasize the use of longitudinal VGs (LVGs) more than ever because of the potential of these devices to increase heat transfer efficiency in thermal systems. The LVGs generate vortices that disrupt the thermal boundary layer and enhance fluid mixing. Therefore, LVGs are considered as one of the effective solutions for improving thermal performance [16-18]. Liu et al. [19] investigated LVGs inside a rectangular microchannel to study the thermal behavior at Re up to 1200. The study reports a heat transfer enhancement of 9-21% for the laminar regime and of 39-90% for the turbulent regime. It was further reported that pressure losses are also found in the ranges of 34-83% for the laminar regime and 61-169% for the turbulent regime. Wang et al. [20] investigated optimizing an LVG in a circular tube under laminar flow. By varying spacing length, central angle, and slice height, significant enhancements in the Nu and f were found. Ebrahimi et al. [21] conducted numerical investigations on rectangular microchannels with LVGs. The analysis considers single-phase laminar flow. Conjugate heat transfer with temperature-dependent thermo-physical properties is taken into consideration. The study shows a 2-25% increase in the mean Nu and a 4-30% increase in the f with LVGs compared to smooth microchannels, over Re = 100-1100.

Various VG geometries, including curved delta winglets, curved rectangular winglets and others, have been analyzed for heat transfer performance in various literature. Zhou and Feng [22] experimentally compared plane and curved winglet VGs of rectangular, trapezoidal, and delta geometries. The study was carried out both with and without punched holes. The curved winglet VGs show

better thermal performance, with lower pressure loss than that of the plane winglet VGs. This was noticed in both laminar and turbulent flow. The curved delta winglet pairs yield a better result. On the other hand, the VGs with punched holes improve thermo-hydraulic performance and reduce the flow resistance. It has been observed that the holes placed at lower and central positions of the VG improve the heat transfer rate and the overall thermo-hydraulic performance. Al-Dulaimi et al. [23] investigated the performance of detached square VGs inside a square duct at Re = 5000. The study varied several parameters such as the blocking ratio, φ, VG number and aspect ratio. The work was carried out numerically using ANSYS Fluent 15. The results indicate that RVGs increase heat transfer by up to 40% due to increased turbulence. A better heat transmission is achieved with the blocking ratio. Thermal performance increases by 17% and 28% for one and three VGs at a blocking ratio of 0.2. At φ =45°, VGs provide an improved heat transfer. However, higher aspect ratios reduce the heat transfer rate.

Mundhe and Bindu [24] investigated the heat response and flow resistance of Conical Offset VGs (COVGs). The study was carried out in a heated steel pipe with turbulent airflow. Numerical simulations were conducted for Re ranging from 4000 to 50000. Both pitch to diameter ratios and φ (15°, 30°, 60°) were varied. A COVG at φ = 60° shows the maximum thermal enhancement. The study reports that the experiment was conducted with different pitches relative to diameter values (1.18, 1.97, 3.94). Nu increased from 3.46 to 6.7 because of increased mixing of the fluid near the wall surface. Zhou and Ye [25] conducted an experimental study on a curved trapezoidal winglet (CTW). It was compared with traditional types of VGs, i.e., rectangular, trapezoidal, and delta winglets. The study reported that the delta winglet performs better both in laminar and transitional flows. However, the CTW shows an improvement in thermo-hydraulic performance in the case of fully turbulent flows. This is due to its streamlined shape and low pressure drop. Parametric study on CTW indicates that smaller φ at 0° and 15° enhances its performance. A greater curvature of 0.5 and a higher inclination angle of 20° enhance its performance. The study also reported that double rows of CTW do not improve thermo-hydraulic performance due to increased pressure drop. Therefore, optimized spacing between the rows is necessary. Gentry and Jacobi [26] performed an analysis of delta wing VGs for flow over a flat plate at low Re. The study showed an increment from 50% to 60% in heat and mass transfer. The optimal delta-wing geometries were identified for various values of Re. Wing chord size was used in the analysis. The results show that stronger vortices formed at the boundary layer border. These vortices pulled the outer flow into the boundary layer and reduced its thickness. Xu et al. [27] investigated thermal behavior in a circular tube with the help of VGs. The flow behavior was also analyzed inside the tube. The study considered various parameters such as φ, blockage levels and a few other related geometric variables. The experiments covered airflows with Re = 6000-33000 under uniform heat input. The findings indicate that heat transfer decreases with pitch ratio. However, it increases with Re, φ and blockage levels. The study showed that heat transfer enhancement is about twice that of the base case. The maximum improvement in thermal performance is 1.45.

Salhi et al. [28] analyzed natural convection in a nanofluid (water with silver or titanium dioxide) in an inclined wavy cavity using FVM. A parametric analysis of variables such as volume fraction, Rayleigh number (Ra), etc., was performed. It was found that the presence of nanoparticles improves heat transfer. The study further reported improved results at higher volume fractions and Ra. The modification of the wavy surface geometry also helps in optimization of thermal performance.

In recent years, researchers have been finding ways to improve heat transfer performance using nanofluids. Many studies apply nanofluids to natural convection systems. These investigations are typically conducted in laboratory flasks to study thermal performance. Chafai et al. [29] studied buoyancy-driven flow of nanofluids in a tilted flat-bottom flask using the FVM. Copper (Cu) and aluminium oxide (Al_2O_3) nanoparticles with various volume

fractions were considered. The results show that Cu nanofluids provide better heat transfer than Al_2O_3 nanofluids, especially at higher nanoparticle volume fractions and Ra. Baiti et al. [30] investigated turbulent mixed convection of a graphene-carbon nanotube hybrid nanofluid inside a round-bottom flask. Thermal performance was found to be impacted by Ra and the nanoparticle volume fraction. However, the agitator speed showed a minor impact. Salhi and Chafai [31] numerically investigated laminar natural convection in a square cavity filled with a water-based hybrid nanofluid containing Ag and Ag-TiO_2 nanoparticles. The cavity featured one heat source and one heat sink with adiabatic walls. The FVM was used to study parameters such as volume fraction of nanoparticles. The type of hybrid nanofluid was also studied. It was found that thermal performance improves when the nanoparticle volume fraction is raised.

Previous studies have investigated the influence of VGs on heat transfer in solar air heaters. These studies show that VGs improve mixing, which in turn increases heat transfer and overall thermal efficiency [32-35]. Alnakeeb et al. [36] investigated a corrugated plate solar air heater fitted with VGs. A 3D numerical model was used to analyze various shapes of VGs, such as rectangular, trapezoidal, and delta-shaped VGs. The study was conducted at various values of φ. The results indicate better thermo-hydraulic performance than that of a corrugated plate alone. Better performance was obtained with RVGs at Re = 7000 and φ = 30°. The study showed that VGs with corrugated plates improve solar air heater efficiency. Hu et al. [37] studied the optimization of solar air heaters by integrating one-eighth sphere VGs into the absorber plate. An electric plate was used to mimic the solar heat input. The study was conducted to find the impact of deflection angle and pitch. Improved performance was achieved at a deflection angle of 180°. A performance factor of 2.03 was also obtained in the study. In comparison to the plain duct, Nu and f are found to increase by factors of 2.45 and 1.96, respectively. The configuration shows an effective method of enhancement for

solar air heaters. Sawhney et al. [38] conducted experiments on a solar heater to study the effect of VGs on thermal performance. The study focused on wavy up delta winglet VGs. It was found that placing the VGs at a suitable location in the fluid domain improves system performance. The study further reported that the thermal performance is best at $\varphi = 60^{o}$. This results in an increase in Nu by approximately 223% compared to a flat plate, with a particular setup at Re = 4000. Tian et al. [39] investigated novel winglet VGs within heat exchangers used for flue gas. It was found that VGs increase surface heat flux by 15.8% and pressure drop by 78.9%, compared to plain fins. Rectangular winglets perform better, increasing surface heat flux by a significant amount. Fahad et al. [40] numerically studied five novel VG shapes in a rectangular channel to improve thermal behavior. The angular orientations of the VGs were also considered in the study.

Recently, studies on VGs with perforations have gained a lot of focus and have been shown to provide enhanced thermal performance. This technique has improved system efficiency by enhancing fluid mixing and flow dynamics. The effects are visible in the system in terms of thermo-hydraulic efficiency and pressure drop characteristics [41-44]. Saini et al. [45] investigated curved delta winglet VGs (CDWVGs), in both perforated and solid forms. The work was done to enhance thermal performance in heat exchangers. Thermo-hydraulic performance across Re = 400-2000 was evaluated with the help of 3D numerical analysis. Among the cases considered, CDWVGs with 6 circular perforations are found to provide the best efficiency. Studies show that modifying the surface of VGs may enhance heat transfer. Kashyap et al. [46] conducted a study on convex and concave surface modifications on both sides of VGs, which resulted in the primary vortex being placed in the right position on the downstream side of the flow, making it stronger than RVG. The cross-sectional area at the vertical belly part was found to be crucial in enhancing heat transfer, while the width towards the upper and lower ends did not affect much. Several concave profiles on the leading side of the VG enhance the heat transfer, whereas convex profiles on the leading and trailing surfaces do not help to improve the thermal performance. Another study introduced modifications to the trailing surface in the form of a step, which increases the intensity of the primary vortex, resulting in increased heat transfer [47]. The VG with a concave semi-circular texture showed the greatest increase in the Nu at 14.4%, while the coefficient of pressure increases by 3.24%. Apart from surface modifications, different modifications, such as an attached surface on the RVG, have enhanced heat transfer significantly. Kashyap et al. [48] numerically investigated on an extended surface attached to the VG. It reported an increase in Nu of 8.9%. The authors [48] indicated that the presence of an additional surface helped to produce stronger vortices with increased shear within the flow, resulting in an improved heat transfer rate.

The literature demonstrates that a suitable modification of VG enhances the heat transfer rate by strengthening vortices. At the same time, extended surfaces are known to improve heat transfer rates. However, detailed parametric studies on VGs with auxiliary surfaces are still limited. Very few studies have analyzed how these auxiliary surfaces affect heat transfer under different configurations. Therefore, this work focuses on the influence of newly designed trapezoidal-shaped auxiliary surfaces on heat transfer. In the current study, the numerical model is initially validated using existing literature data for an RVG fitted on a plate. The primary objective is to explore the effect of four different geometric parameters on thermal and flow behavior of the system. The volumes of the VGs across all the studies are kept constant to facilitate a justifiable comparison. This study focuses on improving heat transfer for a wide range of engineering applications. The new design may help in enhancing the performance of heat exchangers, HVAC systems, car radiators, aerospace cooling systems, power generators, and chemical reactors. It will also offer better cooling for high heat flux components in electronics by disrupting the boundary layer and mixing fluids more effectively.

2. Geometry and formulations

The rate of heat transfer is greatly influenced by the addition of an extended surface. The type and the orientation of the extended surface play an essential role in quantifying the heat rejection rate. In the current study, a VG is placed over a heated surface. Figure 1a shows the schematic diagram of an array of rectangular VGs in a channel with flow between two parallel plates. Owing to the symmetry of the system, the computational domain (Figure. 1b) is selected in a way to accommodate only a single VG over the base plate. To analysis, a computational domain of $L_x \times L_y \times L_z$ is taken into consideration (Figure. 1b). A rectangular vortex generator ($h_p \times l_p \times t_p$) (Figure. 1c) is placed at an angle of φ to the incoming flow over a heated flat plate ($L_x \times L_z$) (Figure. 1b). With an aim to improve the thermal performance of the system, the principal part (PP) of an RVG is modified with the help of an extended auxiliary part (AP) of trapezoidal shape. Figure 1d shows various configuration parameters of such a modified RVG (MRVG). The trapezoidal AP is placed over the PP at a height of h_a. With an angle of ($\alpha_1 = \alpha_2$), the base of the trapezoid is shared with PP, and is same as l_p for all the cases. The other base, the width and the thickness of the trapezoid are taken as l_a, w, t_a.

The thermo-hydraulic performance of a system is commonly evaluated with the help of its various characteristics of temperature and velocity fields. In any fluid and thermal system, the solution of the conservation of the mass, the momentum and the energy equations will pave the way to understand the behavior of parametric fields. Assuming the flow to be laminar, to obtain the velocity and temperature distributions of the system (Figure. 1b), the following general forms of conservation equations are solved [49].

Mass: $$\nabla . \vec{V} = 0 \quad (1)$$

Momentum: $$\frac{\partial \vec{V}}{\partial t} + (\vec{V} \cdot \nabla)\vec{V} = -\frac{\nabla P}{\rho} + \nu \nabla^2 \vec{V} \quad (2)$$

Energy:

$$\rho c_p\left(\frac{\partial T}{\partial t}+(\vec{V}\cdot\nabla)T\right)=k\nabla^2 T \quad (3)$$

Here, the generation of volumetric heat and the radiative mode of heat transfer are neglected. Ignoring the thickness of the bottom plate, the S_y -plane of the computational domain is supplied with heat flux of $|\vec{q}_y|$ (Figure. 1b). The top plate ($S_{y'}$ - plane) is considered to be insulated. Water enters the domain through the S_x -plane with normal velocity V_{in} and isothermal temperature T_{in}. After interacting with the VG, the bottom and the top plate, the fluid leaves through the outlet ($S_{x'}$ -plane) at the atmospheric condition of P_{atm} and T_{atm}. Therefore, a forced convection scenario is achieved over the base plate. The flowing fluid is considered to experience a no-slip condition due to the top and the bottom plates. The S_z and the $S_{z'}$ –planes of the computational domain are considered symmetry for both the velocity and temperature field.

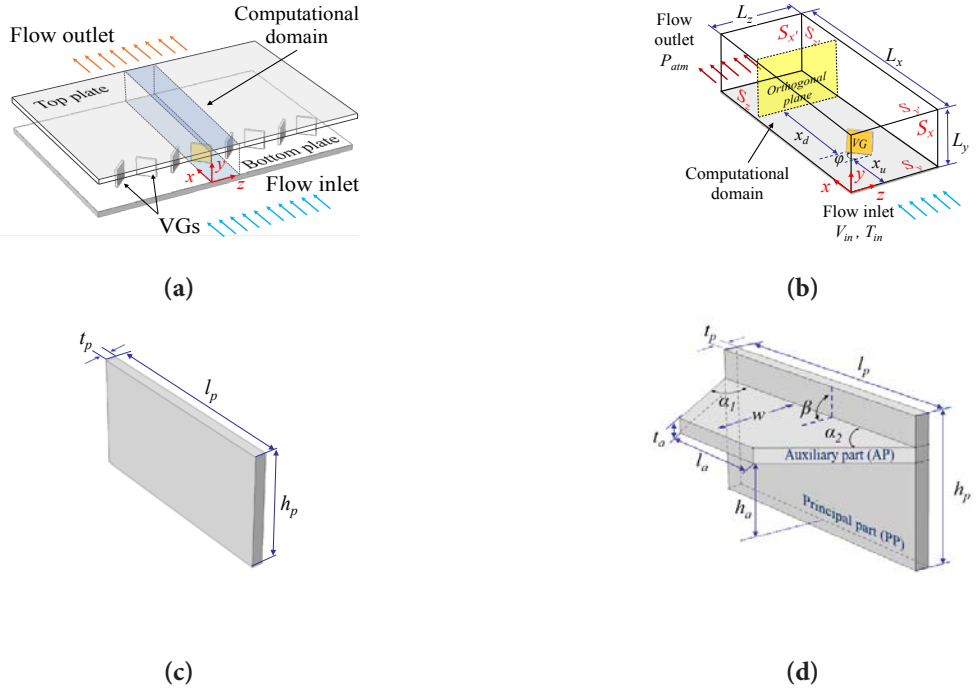

Figure 1. Schematic diagram of **(a)** physical domain with an array of RVGs fitted over a baseplate, and **(b)** the computational domain, **(c)** the RVG and **(d)** the MRVG

In the present work, the governing equations (Eqs. 1-3) are solved using the FVM, with the help of the above-mentioned conditions at the boundary. The ANSYS Fluent 19.2, a commercially available FVM solver is used. Initially, the solver, the governing equations, the boundary conditions, and the considered assumptions are validated using the results of available literature. A grid dependency test is performed prior to the validation work. With the knowledge of u, v, w, and T, from the solution of Eqs. 1-3, various thermo-physical parameters, viz., the Nu, co-efficient of friction C_f, drag coefficient C_d, and thermal performance factor (TPF) η are evaluated. The Nu represents the strength of the convective thermal current in the system. To compare the thermal performance of the various systems considered in the present work, a surface average value of Nu is analyzed and is represented as [49].

$$Nu'' = \frac{h''D_h}{k} \quad (4)$$

The hydraulic diameter D_h of the system is taken as the height of the computational domain L_y [46]. The coefficient of thermal enhancement h" is defined as [49]

$$h'' = \frac{|\vec{q}_y|}{(T_p - T_a)} \quad (5)$$

The Re at the inlet of the flow is evaluated using [49]

$$Re = \frac{\rho V_{in} D_h}{\mu} \quad (6)$$

In a fluid flow system, flow losses are important aspects to characterize the system performance. The nature of flow interaction with the contact surfaces is given by the non-dimensional number known as the surface average skin friction coefficient. Mathematically, it is denoted as [49],

$$C_f = \frac{2\tau_w}{\rho V_{in}^2} \quad (7)$$

The coefficient of drag, or C_d", provides valuable information about the resistance encountered by the VG from the incoming flow. Mathematically, coefficient of drag is expressed as [49],

$$Cd'' = \frac{2F_d}{\rho V_{in}^2 A_v} \quad (8)$$

A system with desirable enhancement in heat transfer rate in comparison to the reduction in frictional flow losses is characterized by the TPF (η). Considering the case of a simple RVG as the reference system, the ratio of the normalized Nu to C_f yields η [47]

$$\eta = \left[\frac{Nu''}{Nu^{ref}}\right]\left[\frac{Cf''}{C_f^{ref}}\right]^{-\frac{1}{3}} \quad (9)$$

where, Nu^{ref} and C_f^{ref} are the surface averaged Nu and C_f for the reference case with the RVG, whereas Nu" and C_f" are the equivalent parameters for the MRVGs.

3. Results and discussion

The present work aims to analyze flow over MRVG under the effect of thermal perturbations in the system. The work is carried out numerically to solve the governing equations (Eqs. 1-3) of the considered physics. Any computational work requires validation of the considered mathematical model. An RVG of dimension ($h_p \times l_p \times t_p$) 0.02 × 0.04 × 0.002 m is placed at an angle (φ) of 45° over the bottom plate (L_x= 1.5 m, L_z=0.06 m) [50]. The height of the computational domain (L_y) is taken as 0.04 m. Water is considered to enter the channel at 293 K (T_{in}) with Re = 350. The incoming fluid leaves the channel through the outlet maintained at 293 K (T_{out}) and atmospheric pressure condition (P_{atm}). The S_y – plane of the domain is supplied with a constant heat flux of 1000 W/m^2. To validate the numerical model, all parameters are considered with reference to Abdollahi and Shams [50]. The considered grid is tested to assess its effect on the results prior to the validation of the numerical solver.

3.1. Solution strategy and grid dependency test

For the conjugate heat transfer problem, the present computational domain is discretized using a staggered grid. The staggered grid helps to obtain the velocity components at the center of the control volume faces. At the same time, the values of pressure and temperature are acquired at the center of the control volumes. A double-precision solver with a higher-order scheme performs the discretization of the governing equations. The first and second-order accuracy are opted for time and space, respectively. To couple the velocity and the pressure terms, SIMPLE algorithm is taken. Further, to discretize the convective terms, a second-order upwind scheme is used. The under-relaxation factors for convergence are 0.3, 0.7, and 1.0 for the pressure, the momentum, and the energy equation, respectively. The convergence criteria for the continuity and the momentum equations are 10^{-4}, and for the energy equation is 10^{-6}, respectively. The above equations are solved using the implicit time-dependent method until the residuals are stabilized at constant values. An appropriate mesh is a requirement to obtain the desired results with good accuracy. Due to the difference in the order of the dimensions of the computational domain and the VG, refinement of the grid is essential. Moreover, the effect of viscosity in the flow domain is mostly realized near the wall. Therefore, refinement of the grid is performed in such zones of the domain. Figure 2a shows the considered mesh in the vicinity of the VG. The grid dependency test is performed using control volumes 2057059, 3029109, 4029643, 5073631, 6047152, and 7981769. Figure 2b shows the effect of the grid on the surface average Nusselt number (Nu"). It has been found that a grid size above 5×10^6, yields a grid independent solution. Hence, in all the upcoming analysis, a grid size above 5×10^6 is used.

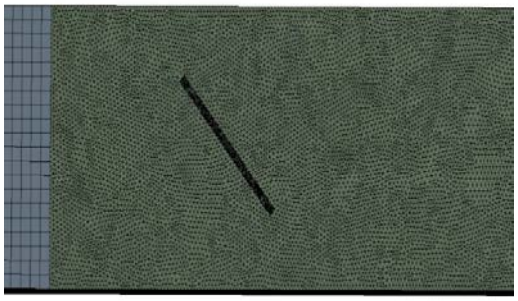

(a)

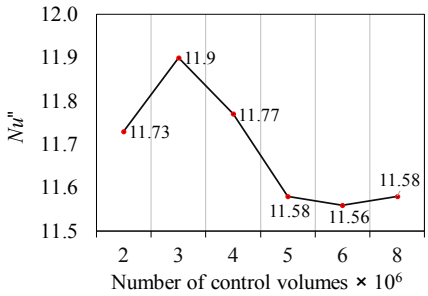

(b)

Figure 2. (a) Generated FVM mesh, and **(b)** effect of grid on Nu"

3.2. Validation

Considering the computational set-up as mentioned by Abdollahi and Shams [50], the validation of the current model is performed using Nu" for various values of φ. Figure 3 shows the variation of Nu" with φ varying from 15° to 75°. Consideration is given to inlet Re of 233 and 350. A maximum deviation of 3.5% is achieved while comparing the results with that of the literature [50]. The surface-averaged Nu, Nu" shows a rising trend as the inlet Re increases. The maximum Nu" is achieved at φ = 45° for Re = 350, as reported by the literature [50]. Figure 3 also shows the value of Nu" for the cases without RVG. Maximum enhancements of 22.8% and 28.4% in Nu" are achieved at Re = 233 and 350, respectively, due to the use of the RVG over the bottom plate.

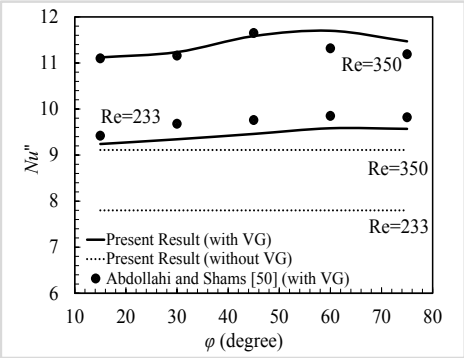

Figure 3. Numerical Validation

To save computational time, the given model is optimized by shortening the length, L_x of the considered system to 1 m. To understand the various geometrical modifications of the vortex generator used in the system, block meshing has been used to get accurate results near the vicinity of the vortex generator. The same set of formulations and boundary conditions have been used to perform the computation. To have a better insight into the thermal and flow dynamics of the system, next, the z-velocity and temperature distribution in various flow sections are analyzed for Re = 350. Figure 4a-d shows the z-velocity contour at various x_d locations. Considerations are given to x_d of 0.005, 0.03, 0.05, and 0.12 m. Figure 4a shows the primary vortex P and high-pressure side horse–shoe vortex HPH. The dotted lines used in P and HPH portray the clockwise (CW) movement. On the other hand, the low-pressure side horse-shoe vortex LPH is an induced vortex, showing an anticlockwise (ACW) movement. It is depicted by the solid lines in the velocity contours. The vortices P and HPH formed induce another vortex, I, in the vicinity of the top plate. It has similar characteristics to those of LPH. At x_d = 0.005 m (Figure. 4a), both P and HPH show good strength. The strength and span of HPH are found to be more than LPH. Figure 4b-d shows the transformation of the vortices. The HPH is losing strength as the fresh flow of fluid comes through the side adjoining the VG. This flow nudges the primary vortex towards the center of the cross-sectional plane, where the offset between the induced vortex and primary vortex reduces. This presses the primary vortex to increase its size and more toward the surface of the plate. It has been observed that the HPH and LPH vortices are nonexistent in x_d = 0.05 m (Figure. 4c). The HPH loses its strength due to the viscous effect, whereas the incoming mass flow of fluid takes out LPH. The centers of both P and I get closer. Further downstream, the span of the P increases, and its center is almost zero offset with the I. The vortex P during its existence disturbs the thermal boundary layer and improves the thermal potential between the plate and the fluid.

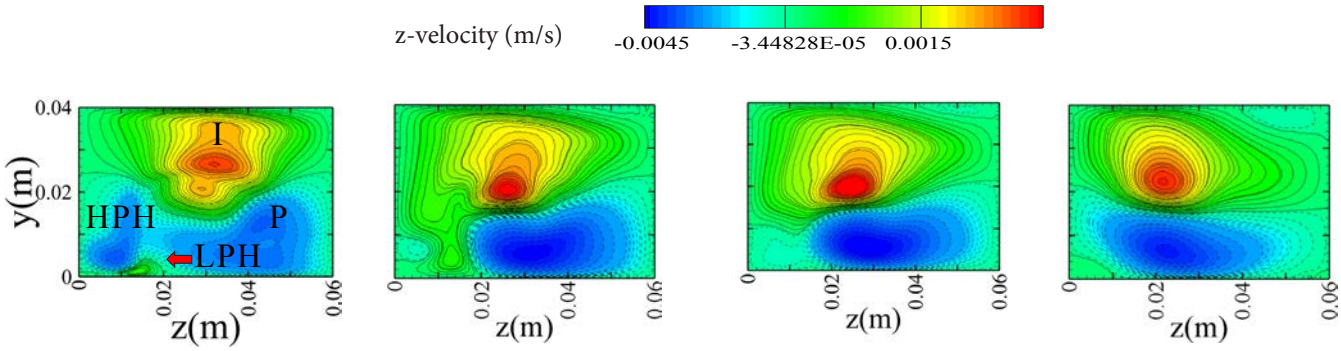

(a) x_d = 0.005 m **(b)** x_d = 0.03 m **(c)** x_d = 0.05 m **(d)** x_d = 0.12 m

Figure 4. Sectional distribution of z-velocity at various flow downstream distances (x_d)

The primary goal of the current work is to improve the system's thermal performance. Understanding the temperature distribution will help in the geometrical modification of the RVG to obtain an improved performance. Figure 5a-d shows the distribution of temperature for a rectangular vortex generator having inlet Re =350. It has been observed that the variation of temperature is limited to a very small thickness away from the bottom plate. Most of the flow Wsection is filled with isothermal fluid at 293 K. With the progression of the flow, as the span of P enhances, more perturbations are introduced in the flow and improve the mixing behavior. This will help the cold layers of fluid in the upper parts of the domain to meet the heated plate. A higher amount of low temperature fluid in the

vicinity of the heated plate increases the temperature gradient. It helps in increasing the convective heat transfer rate. Therefore, compared to a bare plate, a heated plate with RVG improves the thermal performance [50].

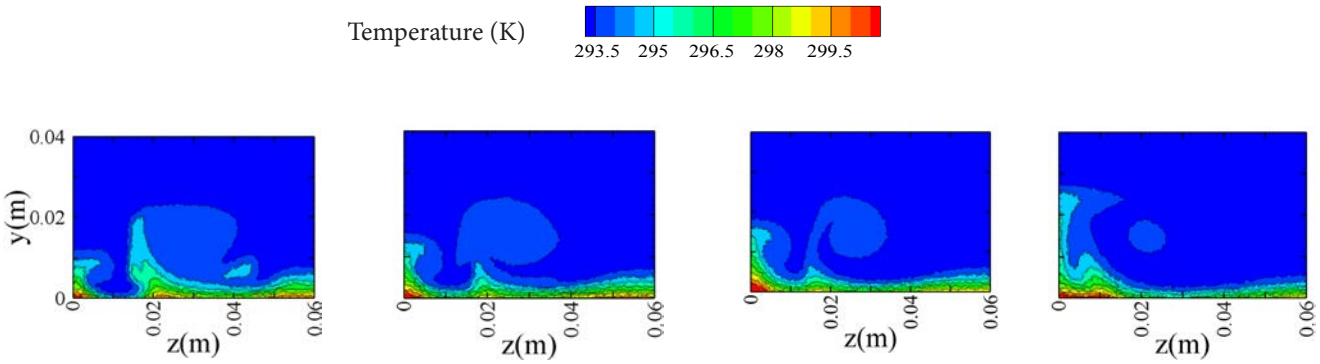

(a) x_d = 0.005 m **(b)** x_d = 0.03 m **(c)** x_d = 0.05 m **(d)** x_d = 0.12 m

Figure 5. Temperature distribution at various flow downstream distance (x_d)

3.3. Modification of RVG

Following the validation of the solver with grid independent solution, next, the consideration is given to the modification of the RVG. With the aim of improving the thermal and flow performance of the system, an auxiliary part (AP) is added to the principal part (PP) of the RVG. The various configuration parameters of the AP and the ranges are presented in Table 1. Considerations are given to four parameters of the AP geometry, viz., the angles α_1, α_2, and β, the width w and the height h_a. As the parameters are varied, to maintain uniform volume of 16×10^{-7} m^3 of the VGs, the thickness of the PP (t_p) and the base (l_a) and the thickness (t_a) of the AP are also varied. To reduce the effect of change in the flow cross-sectional area on the performance parameters of the system, effort is also given to maintain the same projected area (= 5.66×10^{-4} m^2) of the VGs, when viewed from the inlet of the computational domain. However, for the cases with α_1 (= α_2) beyond 90°, the projected area enhances to a maximum value of 3.25%. The MRVG is analyzed by varying geometric parameters. The analysis starts with angles α_1 and α_2, considering $\alpha_1 = \alpha_2$, followed by w, h_a and β.

Table 1. Geometric parameters of the AP and the ranges

Parameter	Range	Unit
$\alpha_1 = \alpha_2$	30 – 150	degrees
w	0.002 – 0.01	m
h_a	0 – 0.0187	m
β	45 – 315	degrees
$t_a = t_p$	0.0013 – 0.002	m

3.3.1. Effect of interior angles of auxiliary surface (α_1 and α_2)

The angles α_1 and α_2 define the projected area of the AP on the xz-plane. This area will be responsible for obstructing flow in the upstream, over the VG. With an aim to obtain an enhanced pressure drop in the flow direction, the current study varies the angles α_1 and α_2 between 30° and 150°. Table 2 shows the various geometric parameters of the MRVG used in this study. It is to be noted that w and β are considered same throughout. However, to maintain uniform volume of the MRVG, the t_a (= t_p) must be varied. It leads to change of h_a.

Table 2. Considered ranges of $\alpha_1 = \alpha_2$ along with variation of other geometric parameters of AP of MRVG

$\alpha_1 = \alpha_2$ (rad)	w (m)	h_a (m)	β (rad)	$t_a = t_p$ (m)
π/6		0.0183		0.0017
π/3		0.0184		0.0016
π/2	0.005	0.0184	*π/2*	0.0016
2π/3		0.0184		0.0016
5π/6		0.0185		0.0015

3.3.1.1. Variation of Nu", C_f" and C_d"

The thermal performance of the system considered is quantified by the dimensionless number Nu. The average value of Nu of the system is evaluated considering the area of the bottom plate. Figure 6a shows a comparison of the Nu" of the configurations having α_1 (= α_2) varying between π/6 and 5π/6. Nu depicts the relative rate of

convection to the conduction heat transfer in the fluid domain. The Nu" is found to increase with angles α_1 and α_2 (Figure. 6a). The behavior of surface average skin friction coefficient (C_f") is also found to follow a similar trend. As the angles α_1 and α_2 are varied from π/6 to 5π/6, the surface area of the AP of the MRVG is found to increase by 56.13%. This increment in area may have resulted in a change in the dynamics of the vortices and it changes the flow behavior over the bottom plate. Due to the modification of the RVG, a maximum rise in Nu" is observed to be 11.13% for the case with α_1 (= α_2) = 2π/3. The corresponding value of the convective heat transfer coefficient h" for the MRVG, which measures the rate of convective heat transfer, is found to be 207.37 W/m^{2}K. Meanwhile, the value of h" for an RVG is 186.59 W/m^{2}K. The C_f" is maximum for case α_1 (= α_2) = 5π/6 with a rise of 5.68%, compared to RVG.

The coefficient of drag C_d" shows the amount of drag experienced by the flow on a normalized scale, due to the presence of the VGs in the flow path. Figure 6b shows the surface averaged drag coefficient C_d" for the cases with α_1 (= α_2) varying between π/6 and 5π/6 and an RVG. Compared to the RVG, an MRVG with α_1 (= α_2) = π/6 shows approximately same value of C_d". However, as the angles α_1 and α_2 increase, the C_d" increases gradually. With 9.43% increment, the MRVG with α_1 (= α_2) = 5π/6 shows the highest value of C_d".

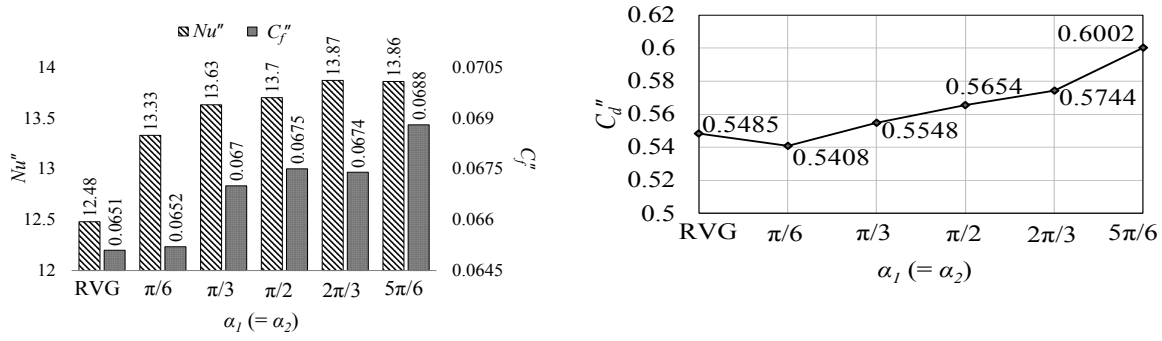

(a) **(b)**

Figure 6. Comparison of **(a)** Nu" and C_f" and **(b)** C_d" of RVG and different MRVGs with angles α_1 (= α_2) varying between π/6 and 5π/6

3.3.1.2. Flow analysis

The modification performed on the RVG is based on the angles α_1 and α_2 showing that the current configuration has the potential to improve the thermal performance of the system. Therefore, an effort is made to understand the flow and thermal behavior of the system by analyzing the velocity and the temperature profiles of the system. Like the previous section, comparative plots of z-velocity and temperature contours are presented in Figures. 7 and 8. Figure 7 shows the sectional distribution of z-velocity at the flow downstream distance (x_d) of 0.005, 0.03, 0.05, and 0.12 m for different cases of MRVGs with various α_1 and α_2. The dynamics of the vortices, as appeared during the propagation of the flow over an RVG are already elaborated in the previous section. Figure 7A.1 - A.4 show the velocity contour of a case of MRVG with α_1 (= α_2) of π/6, at VG downstream distances of 5 mm – 120 mm. It has been found that the presence of the AP of the VG at an angle of π/6 on the leading (high-pressure) surface of the VG leads to the formation of stronger vortex profiles compared to an RVG.

As shown in the figures (Figure 4a and 7A.1), the MRVG yields vortices P and HPH with higher strength and span compared to RVG. The presence of the AP on the PP leads to a change in the shape of the vortex P, with an idle zone of fluid. Due to the similar direction of rotation of the P and HPH, an additional induced vortex I' is created. The I' is visible for the RVG with negligible strength and span. At later stages of the flow, this induced vortex I' starts gaining momentum from I, with the help of P and HPH (Figure 7A.1-E.4). With a higher strength, the HPH always occupies more span compared to the LPH (Figure 7 A.1 and E.1). As the flow progresses, the LPH is positioned to get integrated with the I. Compared to RVG, the LPH and HPH take a little longer to die out (Figure 4b and 7A.2), and it helps in making the P stronger by interacting with it. For all the considered values of α_1 (= α_2) of the MRVGs, the core strength of P is found to be better in strength compared to RVG. For MRVG with α_1 = π/3 (Figure 7B.1-B.4), the sectional velocity distribution is found to be like the case with α_1 = π/6. With identical shapes and changes in the degree of exposure, Figure 7B.2 shows identical vortices and their movements in the flow domain. The primary vortex formed is of higher strength. Compared to the previous cases, a higher strength of P is helpful in enhancing the perturbation near the thermal gradient zone. As the α_1 (=α_2) is increased further, a marginal increase in the span and strength of the P and the HPH are observed at different downstream sectional planes. Figure 7D.1 - D.4 show the z-velocity contours for the MRVG with α_1 = 2π/3. The HPH formed in this case is of higher strength than the earlier cases, which interacts well with the P. This enhances the strength of the P further and helps to interact with the thermal boundary layer

in a better way. Due to a stronger P with the I, an MRVG with α_1 = 2π/3 yields maximum heat transfer compared to RVG. Raising the α_1 (=α_2) beyond 2π/3 to 5π/6 is found to deteriorate the strength of P and I marginally. The HPH also dies out in a little shorter span. The effect is visible in slight reduction in Nu" and increment in C_f" (Figure 6a). However, the current case (α_1 = 5π/6) still yields 11.05% and 5.68% higher Nu" and C_f", respectively, compared to an RVG.

3.3.1.3. Thermal analysis

To understand the effect of the flow on the thermal signatures of the system, the temperature contours are evaluated in the same downstream flow sections of the VG. Figure 8 shows the temperature profiles of the MRVG with considered values of α_1 (=α_2) at a flow section of 0.12 m downstream. The cases of MRVG with various values of α_1 and α_2 are presented in Figure 8a-e. For MRVG with α_1 = π/6, the thermal fonts are enhanced due to the higher strength of the P compared to RVG (Figure 5d). Further, as the values of the angle α_1 (=α_2) are increased, the change in the strength and span of the P with the I, is found to affect the temperature profiles. It has been found that the incorporation of an AP helps in the penetration of colder fluids in the upper region of the domain to reach near the heated plate. This will increase the thermal potential between the plate and the fluid locally and increase the local heat transfer rate. The effect is visible in the change in the Nu". Substantial change is visible between cases with RVG and MRVG with α_1 = 2π/3, which justify the enhancement in Nu".

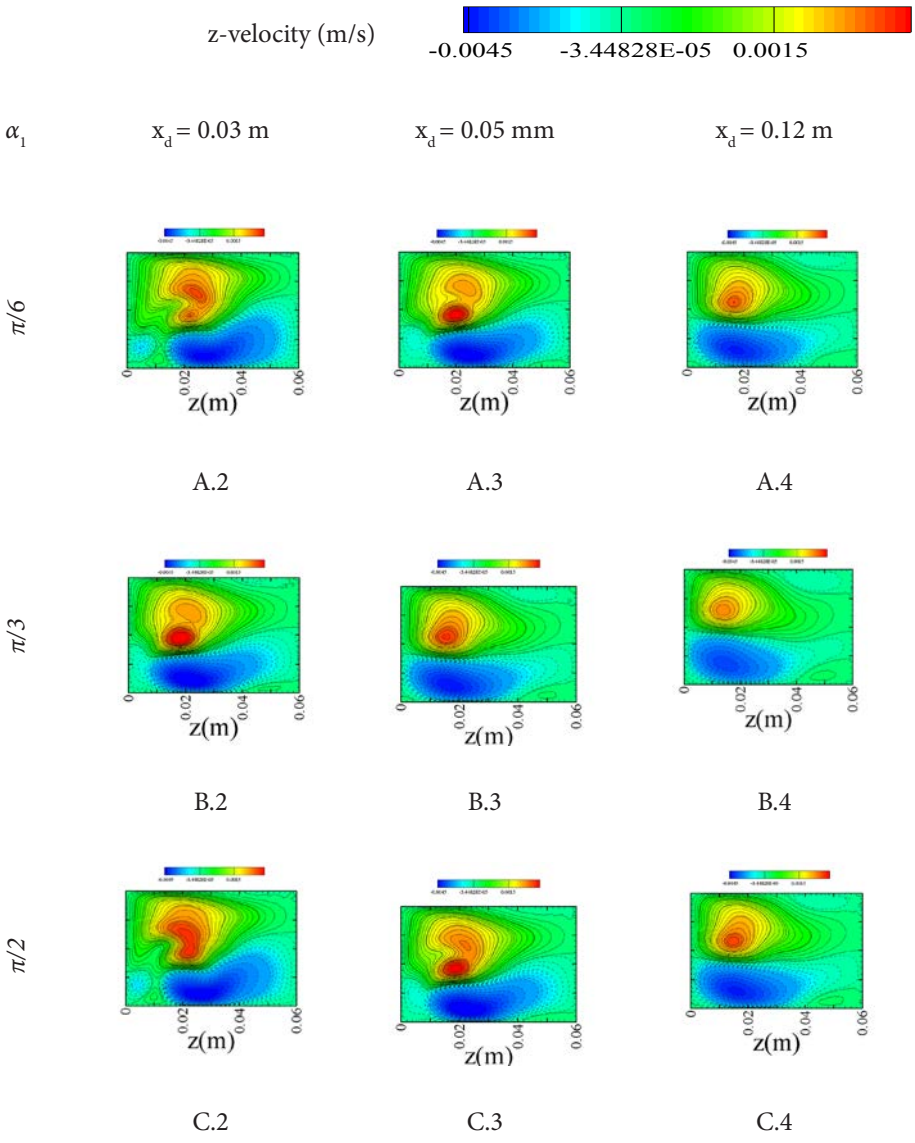

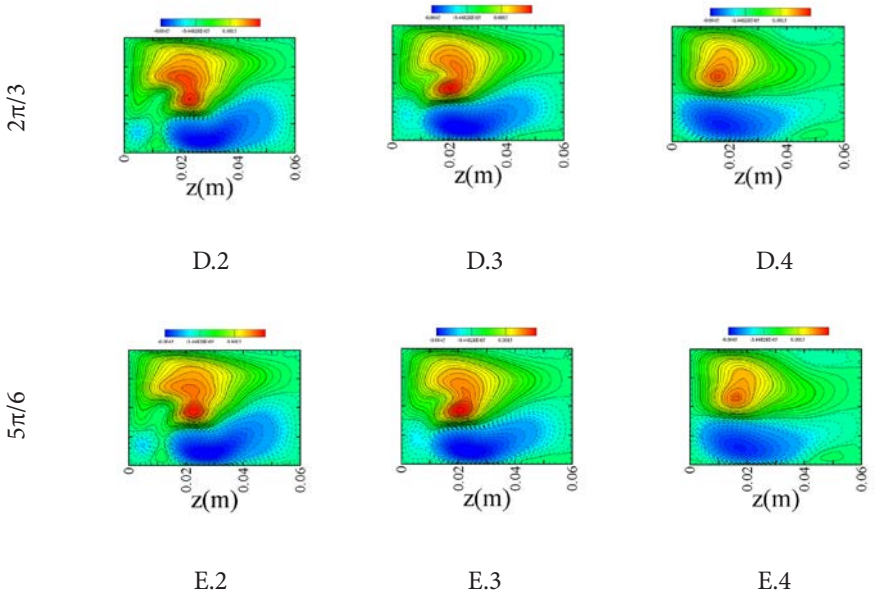

Figure 7. Distribution of z-velocity at different sectional planes downstream of the MRVG with angles α_1 (= α_2) varying from π/6 to 5π/6

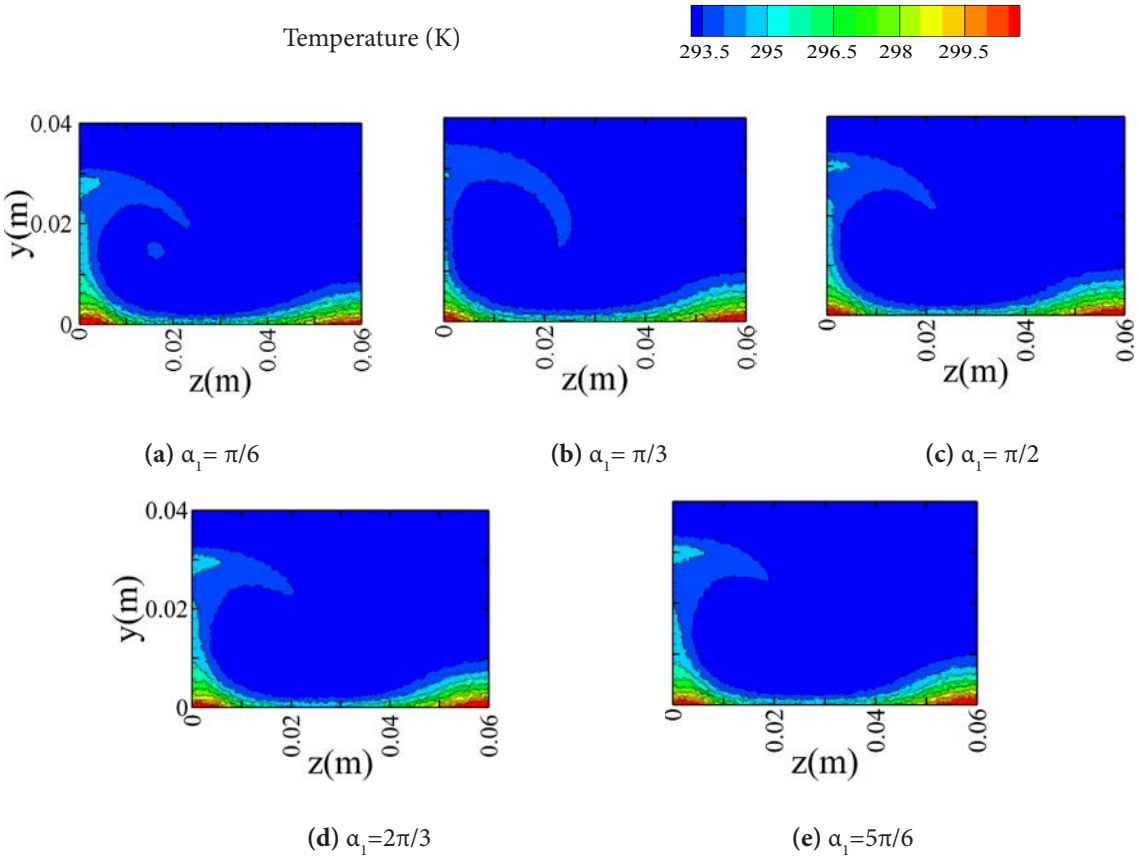

Figure 8. Temperature contours at downstream of the MRVG with α_1 (= α_2) varying from π/6 to 5π/6

3.3.1.4. Variation of η

A thermo-hydraulic system is always limited due to its counteracting behavior of thermal output over flow losses. In any convective system, it is mostly observed that a gain in heat transfer is always compensated with improved flow interaction. Improved flow interaction means more losses. Therefore, to evaluate the overall thermal and flow performance of the system, η (Eq. 9) is considered. Figure 9 shows the comparisons of η for all the above cases of MRVG with reference to RVG.

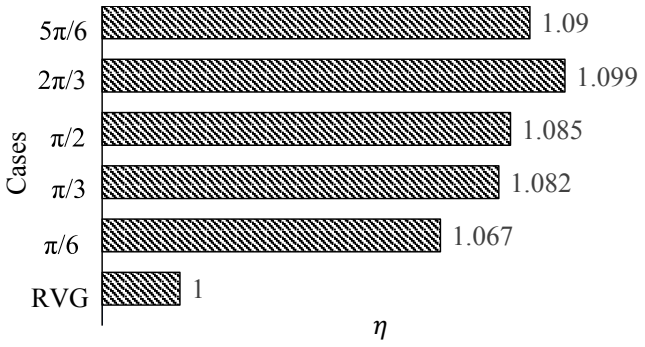

Figure 9. Variation of TPF along the flow over the base plate for different MRVGs

It can be noted that the optimum configuration should have a maximum heat transfer rate with minimum losses. Any value above unity assures improved heat transfer over enhanced flow losses compared to the base case. Compared to RVG, the MRVGs show an improved thermo-hydraulic performance. As the angles α_1 and α_2 increase η also enhances. With a maximum enhancement of 9.9%, the MRVG with $\alpha_1 = 2\pi/3$ shows a stronger nature of vortices, which enhances the heat transfer rate with minimal frictional losses in the system. However, η decreases by a trivial amount for the case of MRVG with $\alpha_1 = 5\pi/6$ due to weaker strength of the primary vortex.

3.3.2. Effect of width of auxiliary surface (w)

With an understanding of the effect of the angles α_1 and α_2 of the MRVG on the thermal performance of the system, next, the width w of the AP is taken into consideration. Considering the case of α_1 and α_2 of $2\pi/3$ having maximum η, the width of the AP is varied from $0.1h_p$ to $0.5h_p$. To maintain the volume of the VG uniform, the t_a (= t_p) is varied, which ultimately affects the h_a. The cases considered are shown in Table 3. It is to be noted that all other dimensions of the system, including the PP of the MRVG are maintained same throughout the study.

Table 3. Considered values of w with other geometric parameters of AP of MRVG

α_1, α_2(rad)	w(m)	h_a(m)	β(rad)	$t_a = t_p$(m)
2π/3	$0.1h_p$	0.0182	π/2	0.0018
	$0.2h_p$	0.0183		0.0017
	$0.3h_p$	0.0185		0.0015
	$0.4h_p$	0.0186		0.0014
	$0.5h_p$	0.0187		0.0013

3.3.2.1. Variation of Nu", Cf" and Cd"

The width, w, of the MRVG is responsible for increasing the surface area of the AP. As seen in the previous section, the AP blocks the upstream flow over the top surface of the RVG. Therefore, it is expected to have a higher pressure drop along the flow direction. A higher pressure drop in the flow direction improves the strength of the P and HPH and will ultimately improve the heat transfer rate. With this key idea, various cases of the MRVG with different values of w are simulated. Figure 10a shows the variation of Nu" and C_f" for the considered cases.

It has been observed that as the w increases from $0.1h_p$ to $0.5h_p$, both Nu" and C_f" increase. Compared to RVG, a rise of 1.28%, 6.65%, 13.62%, 19.79%, and 27.16% in Nu" are observed for MRVG with w of $0.1h_p$, $0.2h_p$, $0.3h_p$, $0.4h_p$ and $0.5h_p$, respectively. The corresponding values of h" are found to be 188.98 W/m^{2}K, 198.99 W/m^{2}K, 212 W/m^{2}K, 223.51 W/m^{2}K, and 237.27 W/m^{2}K. A higher convective heat transfer coefficient (h") indicates more efficient convective heat transfer between the surface and the fluid. At $w=0.5h_p$, the maximum heat transfer is achieved. Following a similar trend to that of h" and Nu", the C_f" rises for the system by 1.08%, 3.07%, 5.22%, 7.07%, and 11.98%, respectively. A higher interaction of the flow with the active area in the current study leads to a higher heat transfer rate. Compared to RVG, the increment in w of the system increases the surface area of the MRVG by a maximum value of 51.39%, in the current study. This increment in area is found to affect the drag experienced by the flow in the domain. Figure 10b shows the variation of C_d" for the considered cases. A rise in C_d" by 1.6%, 3.7%, 6.51%, 10.15%, and 14.13%, are observed for MRVG with w of $0.1h_p$, $0.2h_p$, $0.3h_p$, $0.4h_p$ and $0.5h_p$, respectively. To understand the effect of w on the flow behavior, the z-velocity contours at different downstream flow sections are evaluated, next (Figure 11).

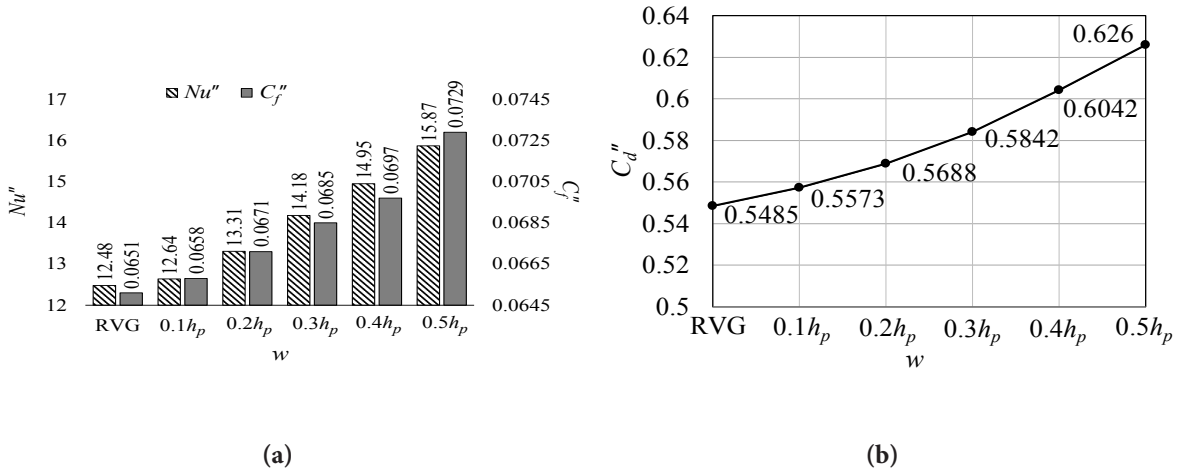

Figure 10. Comparison of **(a)** Nu" and C_f" and **(b)** C_d" of RVG and different MRVGs with varying w

3.3.2.2. Flow analysis

Figure 11 shows the z-velocity distribution of various cases of MRVG with w of $0.1h_p$ - $0.5h_p$. The velocity contours are presented at a flow section located downstream distances from VG, as mentioned earlier. In Figure 11A.1-A.4 for the cases with w=$0.1h_p$, HPH and LPH are seen to have improved strength compared to RVG (Figure 4a-d), which interacts with the P. Figure 11B.1-B.4 shows the case with w = $0.2h_p$, where a higher strength HPH compared to RVG and w = $0.1h_p$ appears at x_d = 30 mm. This HPH interacts with the P and strengthens it in the flow downstream, which further helps in better interaction of the flow with the bottom plate. For cases with w > $0.2h_p$ (Figure 11C.1 - E.4) two prominent induced vortices I and I' are observed. These two induced vortices, almost of equal strength, interact with each other for a distance longer than x_d = 50 mm. Hence, the induced vortices occupying more space in the cross-section push the P near the bottom plate with greater strength. Thus, the squeezing effect helps in increasing the heat transfer rate. As the flow progresses, unlike earlier cases, the HPH, too, does not die out quickly and tends to keep interacting with other vortices. These interactions are responsible for increasing the C_f". A steady rise in the heat transfer rate has also been noticed with an increase in w in this study (Figure 10a).

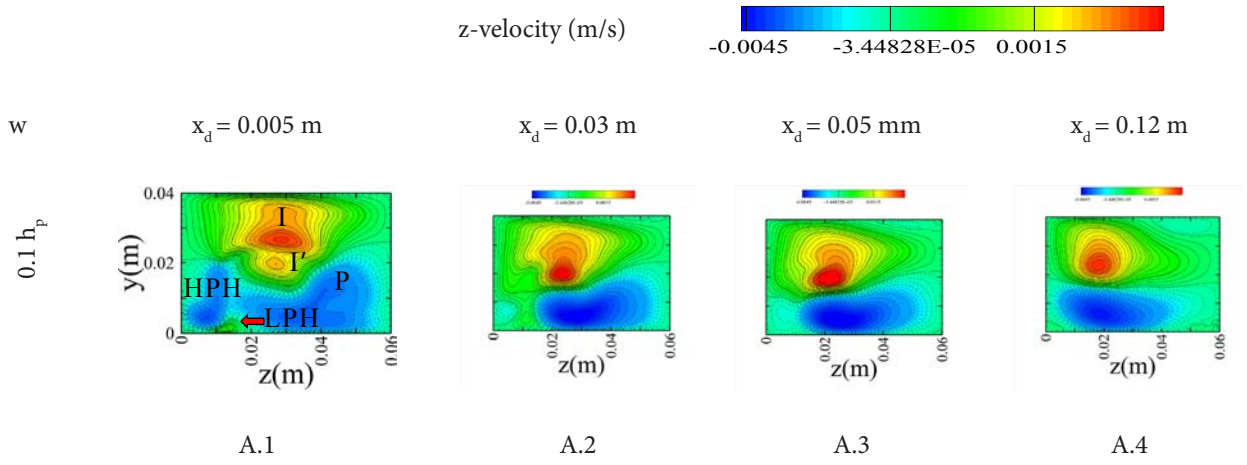

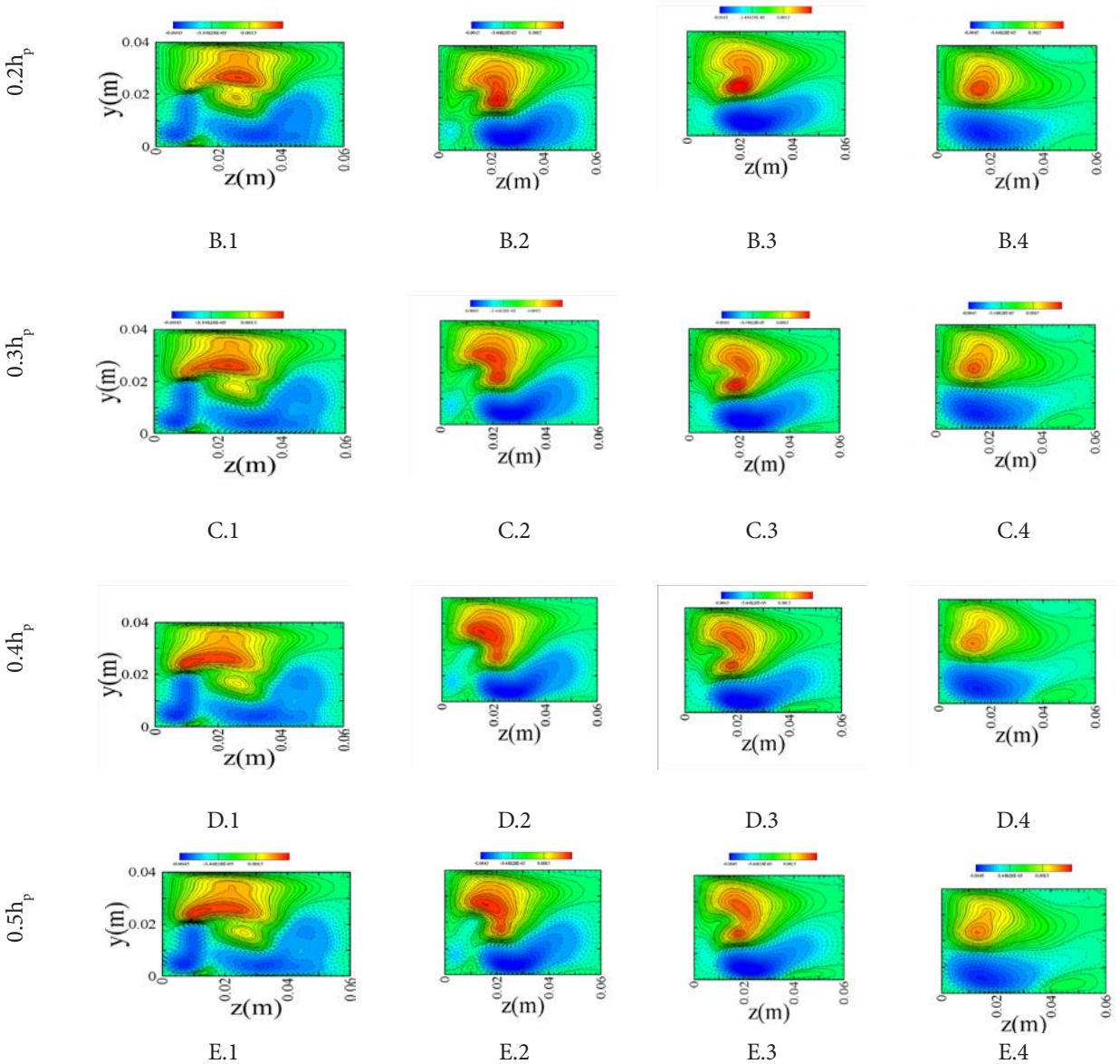

Figure 11. Distribution of z-velocity at different sectional planes downstream of the MRVG with w varying from $0.1h_p$ to $0.5h_p$

3.3.2.3. Thermal Analysis

Following the analysis of velocity distribution, the thermal signatures due to MRVGs are presented in Figure 12a-e. The temperature profiles of the considered cases are at the flow section located at 0.12 m downstream of the VG. It is clear from the temperature profiles that the MRVGs show a lower concentration of temperature fonts near the bottom plate. Low temperature fluid in the vicinity of the heated bottom plate yields a higher temperature gradient. This will help in obtaining a higher heat transfer rate. Figure 12a shows the temperature profiles for the case of MRVG with w = $0.1h_p$. The obtained temperature distribution is found to be better than that of RVG (Figure. 5d). As the MRVGs yield vortices of better strength compared to RVG, better mixing of fluids helps in mixing of fluid at different temperatures. Therefore, MRVGs with w= $0.1h_p$ – $0.5h_p$ show a better heat transfer rate, which is reflected in Nu" (Figure 10a). As w increases, the improvement in the performance of the vortices yield improved temperature distribution. Hence, the Nu" is increased with increasing values of w (Figure 10a).

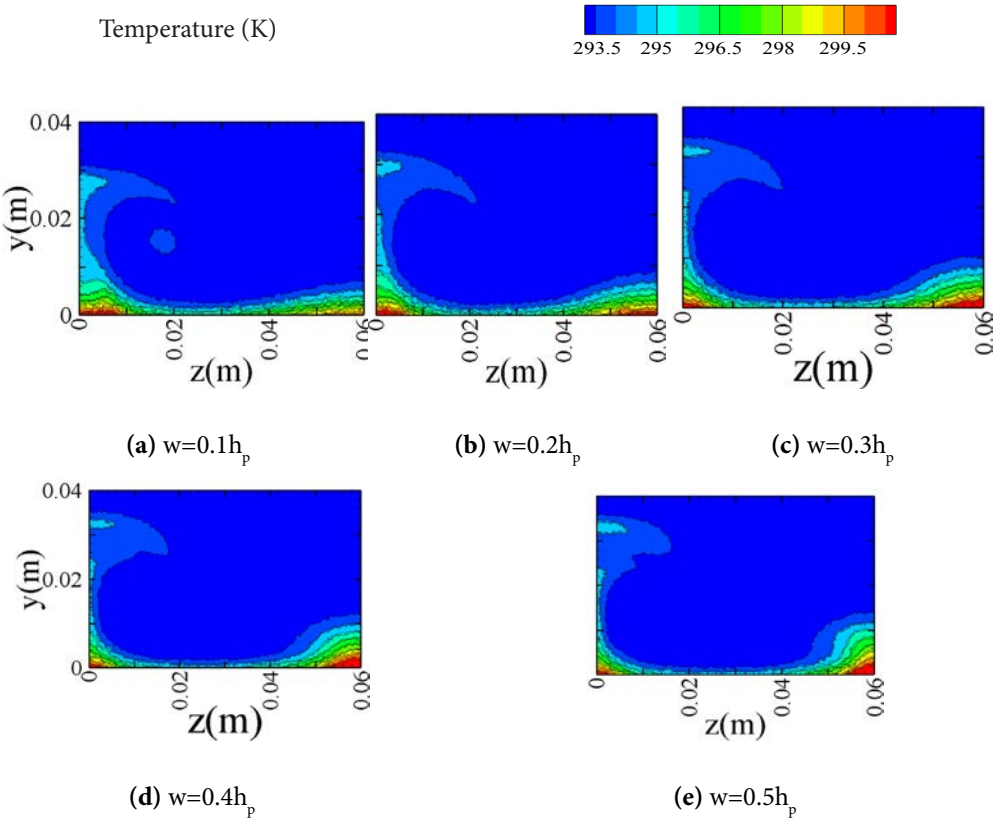

Figure 12. Temperature contours downstream of the MRVG with w varying from $0.1h_p$ to $0.5h_p$

3.3.2.4. Variation of η

An overall idea of the heat transfer and performance of the flow in the system can be described by η. The values of η for all the considered cases are shown in Figure. 13. As w increases, the interaction of the flow with the heat transfer surface increases. Therefore, the flow losses of the system increase along with the enhancement in the thermal performance of the system. The net effect is an enhancement in the values of η with an increase in w. Compared to the RVG, all the cases of MRVG show improvement in the η. The MRVG with w = $0.5h_p$, shows 22.4% improvement in η compared to an RVG. From the results, it is seen that the width w of the AP always has a favorable effect. Without any geometrical constraint in modelling the MRVG, it is possible to achieve higher values of the performance parameters of the system.

Figure 13. Variation of η for RVG and MRVGs with w

3.3.3. Effect of position of AP (ha)

The position of the AP on the PP is expected to influence the flow behavior downstream of the VG by affecting the pressure drop in the flow direction. Therefore, with the variation of the angles α_1 and α_2, and width w of the AP, the height h_a is taken into consideration next. From the previous study, it has been observed that for $\alpha_1 = \alpha_2 = 2\pi/3$ and $w = 0.5h_p$, the MRVG yields maximum thermal and flow performance (η). Following these parameters, the height h_a is varied from 0 to $0.935h_p$ (Table 4). To maintain uniformity in the volume of the MRVG, the t_a and the t_p are taken as 1.3 mm, and the angle β is maintained at $\pi/2$.

Table 4. Considered ranges of h_a along with variation of other geometric parameters of AP of MRVG

α_1, α_2 (rad)	$2\pi/3$
w (m)	$0.5h_p$
h_a (m)	0, $0.25h_p$, $0.5h_p$, $0.75h_p$, $0.935h_p$
β (rad)	$\pi/2$
$t_a = t_p$ (m)	0.0013

3.3.3.1. Variation of Nu", Cf", and Cd"

Figure 14a shows the variation of Nu" and C_f" with h_a. It has been observed that for the AP located at a height (h_a) of 0, $0.25h_p$, $0.5h_p$ and $0.75h_p$, the Nu" reduces, even if the flow interaction (C_f") with the MRVG increases (Figure. 14a). With the AP located at the top location ($0.935h_p$), the MRVG can surpass the RVG in terms of Nu" and C_f" by 27.16% and 11.98%, respectively, with the highest h" measured at 237.27 W/m^{2}K for this location. For h_a of 0, $0.25h_p$, $0.5h_p$, and $0.75h_p$, the Nu" reduces by 5.38%, 8.01%, 8.09%, and 0.64%, respectively, whereas the C_f" enhances by 0.46%, 2.61%, 3.38% and 3.07%, respectively. In a similar line, the C_d" also enhances by 1.75%, 1.73%, 3.04%, 2.18%, and 14.12%, respectively.

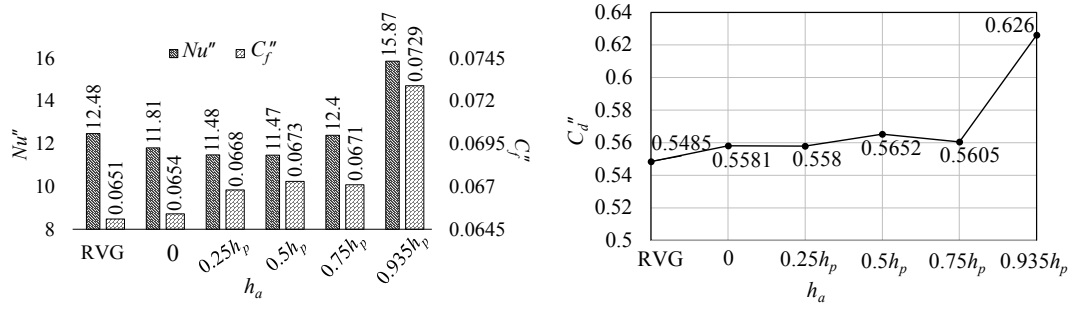

Figure 14. Comparison of **(a)** Nu" and C_f" and **(b)** C_d" of RVG and different MRVGs with varying h_a.

3.3.3.2. Flow analysis

The change in the thermal and flow behavior of the considered cases with different h_a are best understood from the process of vortex formation inside the flow domain (Figure 15). Figure 15 A.1-A.4 shows the velocity distribution for the case with AP located on the PP touching the base plate, where horse-shoe vortices such as HPH and LPH have poorer strength. As the flow progresses, LPH dies out quickly due to the continuous flow of fluid around the VG. However, vortex HPH tried to interact well with the P, but due to poor strength and viscous effect, it died out early as well. The P, formed as the flow progresses, is of poor strength, giving lower heat transfer rates. For the AP located at $0.25h_p$ (Figure 15B.1-B.4), HPH starts right on top of LPH, which is attached to the surface of the plate. With the progression of the flow, HPH dies out earlier than in the previous case ($h_a = 0$). The LPH starts interacting with the P. However, the vortex P loses its strength as the flow progresses and contributes less to the heat transfer process compared to the previous case. Figure 15C.1 - C.4 shows the velocity distributions of the case with AP located at $0.5h_p$, where two HPH and LPH are created. The LPH attached to the bottom plate is of poorer strength. The P, and the I, are observed to strengthen with the progression of the flow and is of similar strength to the case with AP located at $0.25h_p$. Therefore, the heat transfer characteristics are also found to be similar in nature (Figure 14a).

For the AP located at $0.75h_p$, (Figure 15D.1-D.4), the vortices formed are stronger than in earlier cases. Compared to RVG, both HPH and LPH die out early, with almost of similar nature to P and I. This yields a moderate enhancement in heat transfer rate compared

to the cases with h_a = 0, 0.25h_p, and 0.5h_p. Figure 15E.1-E.4 show improved characteristics of the vortices for the AP positioned at 0.935h_p, as compared to the earlier cases. The HPH produced is of higher strength, whereas the vortex I, with better strength and span, squeezes the P against the bottom plate. This phenomenon improves the interaction of the flow with the heat transfer surface, and the thermal performance of the system increases. It has been observed that at the downstream of the VG, the structure of the vortex formation is almost similar for most of the cases, with minor differences in the sections at x_d = 0.005 m. Therefore, the focus is diverted to the upstream of the VG. At the upstream, the velocity gradient in the y-direction contributes to the formation of a longitudinal vortex. This vortex is made visible by filtering out the velocity vectors having the positive direction of flow.

Figure 16 shows the formation of a longitudinal vortex in the xy-plane located at z = 0.03 m, close to the heat transfer surface. It has been observed that the span and strength of the vortex reduce as the RVG is modified with an AP touching the base plate (Figure 16a and b). It is to be noted that the AP, along with the PP surfaces, are not directly participating in heat transfer process. Therefore, the produced vortex touching the top surface of the AP does not promote any heat dissipation (Figure 16b). As the height of the AP is changed to h_a= 0.25h_p and 0.5h_p, this longitudinal vortex does not form due to appearance of the stagnation point on the AP close to the bottom wall (Figure 16c and d). As the h_a is increased to 0.75h_p the stagnation point on the AP moves away from the bottom wall, and the longitudinal vortex reappears with strength and span close to that of RVG (Figure 16e). For the AP located at maximum height (0.935h_p), the span and the strength of the vortex improves (Figure 16f). Hence, a rise in the heat transfer rate has been observed with increment in Nu".

3.3.3.3. Thermal analysis

The current aim of the study is to enhance the thermal profile of the system. After analyzing the velocity profiles of the abovementioned cases, the thermal profiles are studied next. Figure 17 depicts the related isotherms of all the cases at the flow section located at 0.12 m downstream of the VG. Improvement in the heat transfer rate of the system requires a higher temperature gradient. Figure 17a shows the thermal fonts for the case with AP located at the bottom of the PP. The temperature distribution for this case is observed to be of similar nature, compared to the RVG (Figure 5d). When the AP is moved to 0.25h_p and 0.5h_p (Figure 17b and 17c), fluid having a higher temperature rises above the base plate. However, there is an accumulation of high temperature fluid near the bottom plate. It is due to the poor formation of the primary vortex P with lesser strength, as compared to RVG. As the AP is moved to 0.75h_p (Figure 17d), the temperature distribution is found to improve. However, due to the higher rate diminishing of the P in this MRVG, it could not surpass the performance of the RVG. As observed (Figure 17e), the AP located at maximum h_a yields a temperature distribution with better penetration of the free stream fluid in the vicinity of the bottom plate. Hence, a higher temperature gradient is obtained, which results in improved Nu" compared to an RVG.

3.3.3.4. Variation of η

Considering the RVG as a reference, Figure 18 shows the variation of η with a change in h_a. The MRVGs with AP located at 0, 0.25h_p, 0.5h_p and 0.75h_p show thermo-hydraulic performance less than unity (Figure 18). It means that these configurations show higher flow losses with respect to the change in Nu". However, when the AP is placed at the maximum height (0.935h_p), it shows 22.4% improvement in η as comparison to an RVG. Therefore, from the above study, an MRVG with $\alpha_1 = \alpha_2 = 2\pi/3$, w = 0.5$h_p$, h_a = 0.935h_p, and $\beta = \pi/2$ is found to be the best possible configuration (Figure 1d). To improve the performance of the MRVG further, the angle of inclination β of the AP is considered for study.

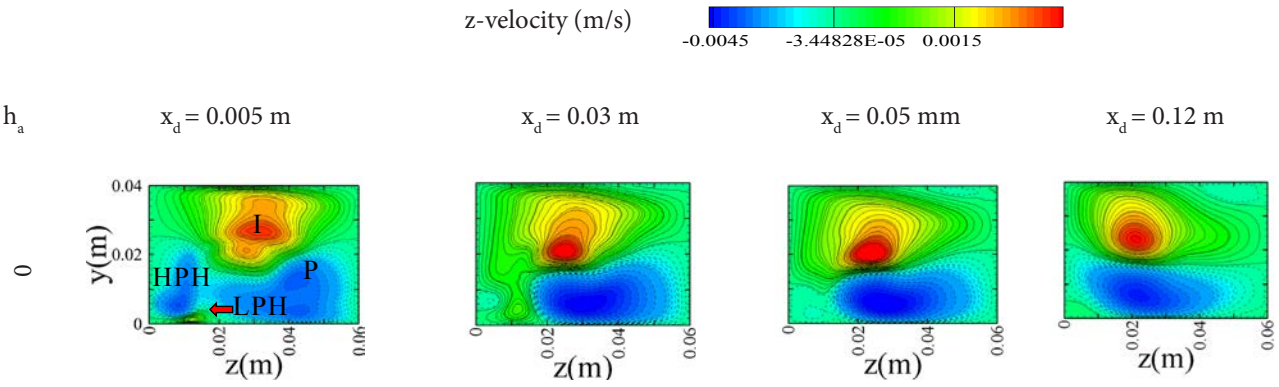

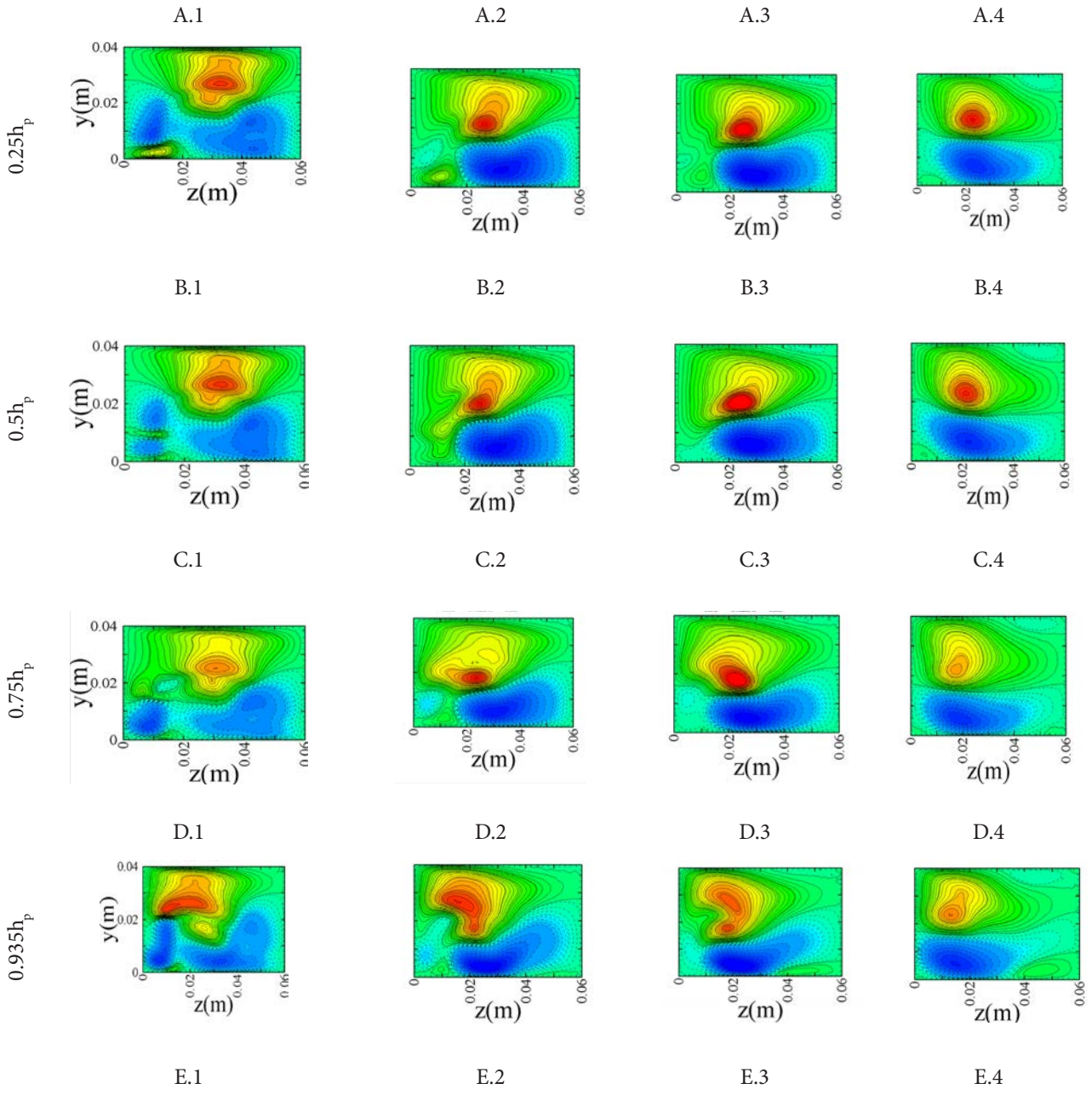

Figure 15. Distribution of z-velocity at different sectional planes downstream of the MRVG with h_a varying from 0 to $0.935h_p$

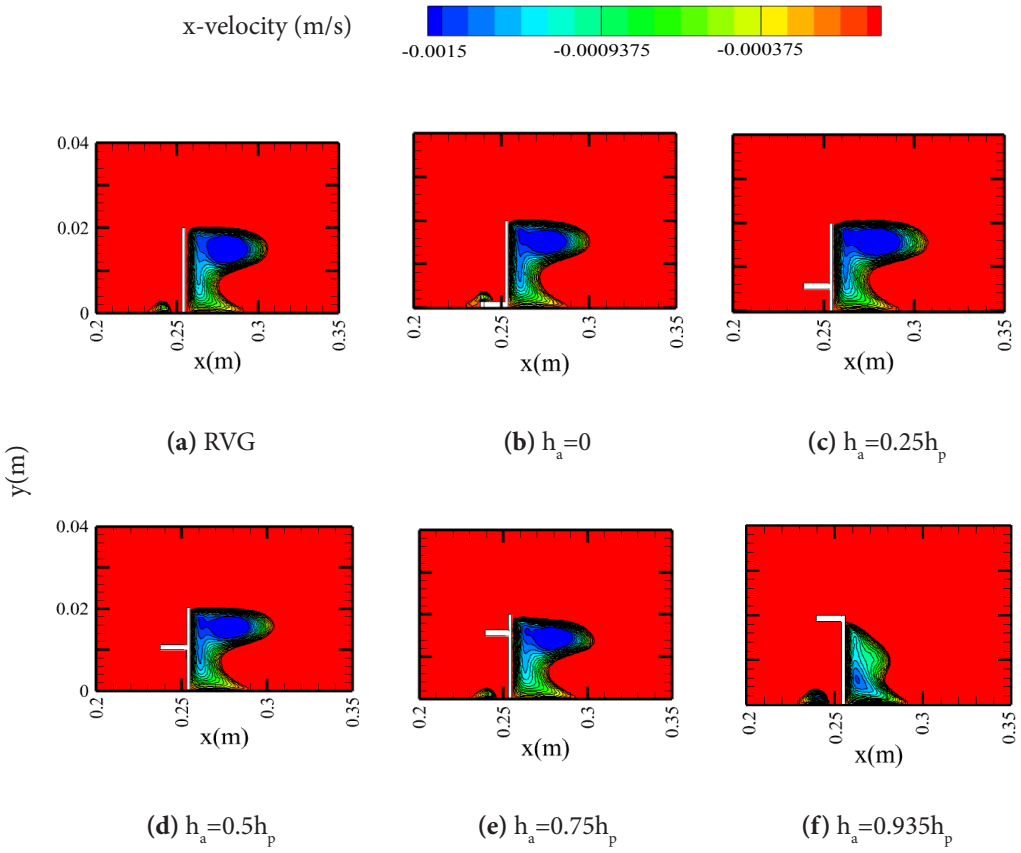

Figure 16. Formation of longitudinal vortex upstream of the VG for AP located at various heights on PP

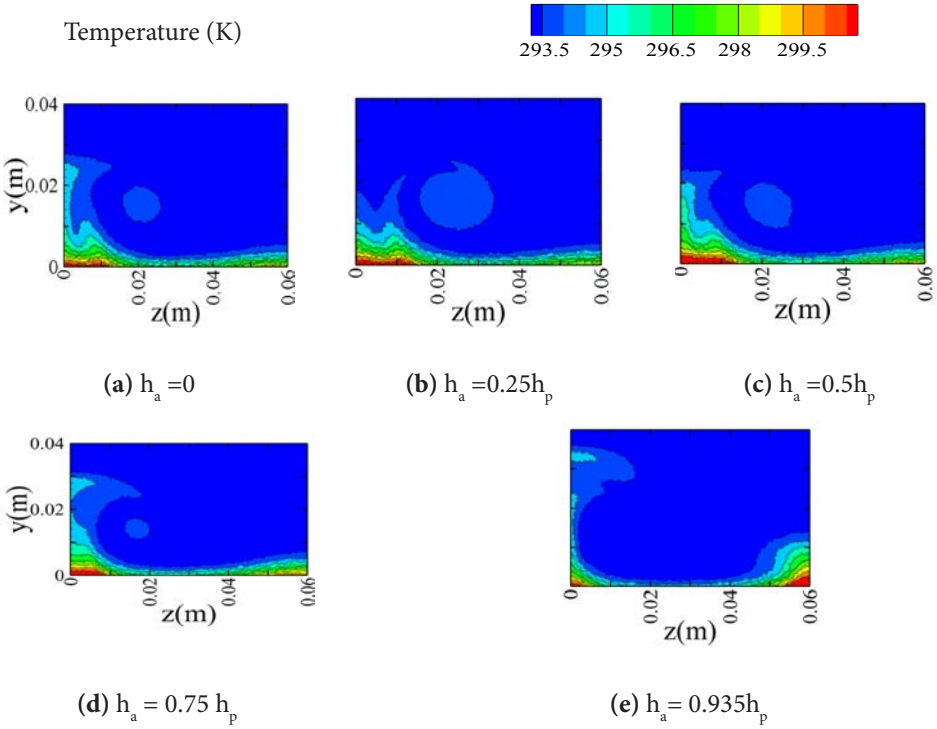

Figure 17. Temperature contours downstream of the MRVG with h_a varying from 0 to $0.935h_p$

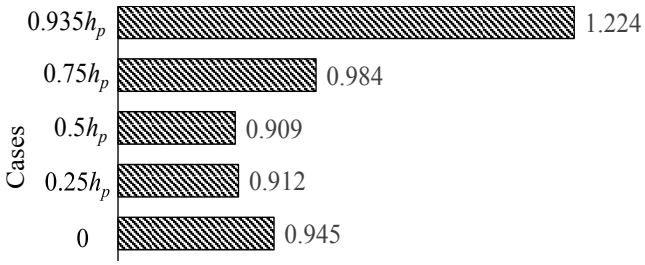

Figure 18. Comparison of η of RVG and different MRVGs with height h_a varying between 0% h_p and 93.5% h_p

3.3.4. Effect of angle of inclination of auxiliary surface with principal surface (β)

The AP placed on the PP of the MRVG is responsible for blocking the upstream flow above the VG. This hindrance to the flow creates a pressure drop along the flow direction, across the VG. Pressure drop in such cases has a favorable effect on the vortex strengths and improves the heat transfer. With this insight, the effect of angle β between the AP and PP is studied in this section. The work is carried out using $0 < \beta < 2\pi$, with a step size of $\pi/4$, considering all other parameters constant (Table 5). For the ease of discussion, the considered cases may be divided into sets with $0 < \beta < \pi$ and $\pi \leq \beta < 2\pi$.

Table 5. Considered ranges of β along with variation of other geometric parameters of AP of MRVG

α_1, α_2 (rad)	w (m)	h_a (m)	β *(rad)*	$t_a = t_p$ (m)
2π/3	0.5h_p	0.935h_p	π/4, π/2, 3π/4, π, 5π/4, 3π/2,7π/4	0.0013

3.3.4.1. Variation of Nu", Cf" and Cd"

The mass movement of the working fluid inside the computational domain is responsible for the dissipation of thermal energy from the bottom plate. It is further controlled using the strength and span of the formed vortices in the upstream and downstream of the VG. Figure 19a shows the variation of Nu" for various cases of β. For $\beta = \pi/4, 3\pi/2$ and $7\pi/4$, the Nu" almost remains the same as compared to RVG. However, all other cases show a rise in the value of Nu". Compared to RVG, the Nu" rises by 27.16%, 27.64%, 13.06%, and 7.05% for $\beta = \pi/2, 3\pi/4, \pi$ and $5\pi/4$, respectively. The corresponding values of h" are found to be 237.27 W/m^{2}K, 238.17 W/m^{2}K, 210.96 W/m^{2}K, and 199.74 W/m^{2}K respectively. Following a similar trend to that of Nu", the flow losses (C_f") in the system also closely matches with that of the RVG for $\beta = \pi/4, 3\pi/2$ and $7\pi/4$ (Figure 19a). In the MRVGs with $\beta = \pi/2, 3\pi/4, \pi$ and $5\pi/4$, the C_f" values rises by 11.98%, 20.58%, 28.87% and 17.82% indicating higher flow resistance experienced by the fluid. As the angle β increases to a value of *π, the MRVG occupies the maximum of the flow cross-section and behaves* as a single RVG having a height 1.5 times that of the original RVG considered in the study. The increased height in this case ($\beta = \pi$) blocks the flow cross-section to a maximum extent compared to all other cases of MRVG. Therefore, the MRVG with $\beta = \pi$ yields a maximum rise in C_f" of 28.87%. The maximum flow losses in the system in this case is a result of reduction in flow section, which could not be utilized to improve the flow characteristics. Therefore, regardless of highest C_f", the Nu" has improved slightly. The C_d" also shows a similar trend (Figure 19b). To understand the interaction of the heated surface with the flow, the velocity contours at various sections are presented next.

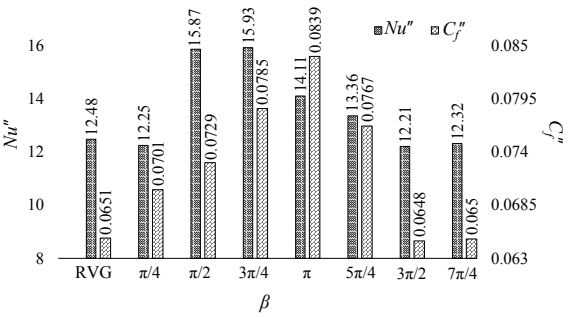

(a)

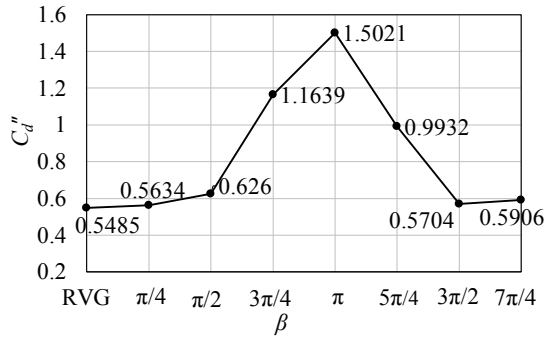

(b)

Figure 19. Comparison of **(a)** Nu" and C_f" and **(b)** C_d" of RVG and different MRVGs with β varying between π/4 and 7π/4

3.3.4.2. Flow analysis

Figure 20 and 21 presents the z-velocity contours of the cases with $0 < \beta < \pi$ and $\pi \leq \beta < 2\pi$, respectively, at various flow sections. Figure 20A.1-A.4 shows the formation of vortices for $\beta = \pi/4$. The formed vortices, in this case, are almost of the same strength compared to the RVG (Figure 4a-d). As the angle β is increased to $\pi/2$ (Figure 20B.1-B.4), the strength of the HPH and the LPH increases. The primary vortex P also shows an improved strength and contacts with the bottom plate initially. However, as the flow progresses, both P and I start losing their strength. The I, in this case, shows two vortex cores with increased span at $x_d = 0.05$ m. It pushes the primary vortex P more towards the bottom plate and disrupts the boundary layer near the heated surface. As the angle β of the AP becomes $3\pi/4$, *the* former P and HPH immediately after the VG ($x_d = 0.005$ m) show an indistinct profile (Figure 20C.1-C.4). However, as the flow progresses, the P, combined with HPH, yields vortices of higher strength and distinct zones of appearance. The LPH, in this case, is of weaker strength compared to RVG. The enhanced I, of superior strength compared to all previous cases, squeezes the vortex P on the base and helps to improve the thermal performance of the system.

At angle $\beta = \pi$, the MRVG occupies the maximum cross-sectional area of the flow section. This leads to exposure of the maximum projected area of the MRVG with maximum blockage in the channel. Figure 21A.1-A.4 shows the vortex formation downstream of the VG. Interestingly, in this case, I try to move underneath the P and to move it away from the heated surface. The P is also observed to hover away from the bottom plate compared to previous cases. As the P reaches $x_d = 0.12$ m, the vortex is observed to split and lose its strength. This reduction in strength leads to reduced thermal performance compared to $\beta = 3\pi/4$. The case with $\beta = 5\pi/4$ (Figure 21B.1-B.4) also shows similar behavior of the vortices downstream of the VG. Therefore, the flow in this case interacts with the heated surface in a similar manner and yields a Nu" close to that in the case $\beta = \pi$. For cases $\beta = 3\pi/2$ and $\beta = 7\pi/4$ (Figure 21C.1-C.4 and D.1-D.4), the former vortices are observed to be lower in strength compared to the earlier cases. This results in poor thermal interaction with the heated plate.

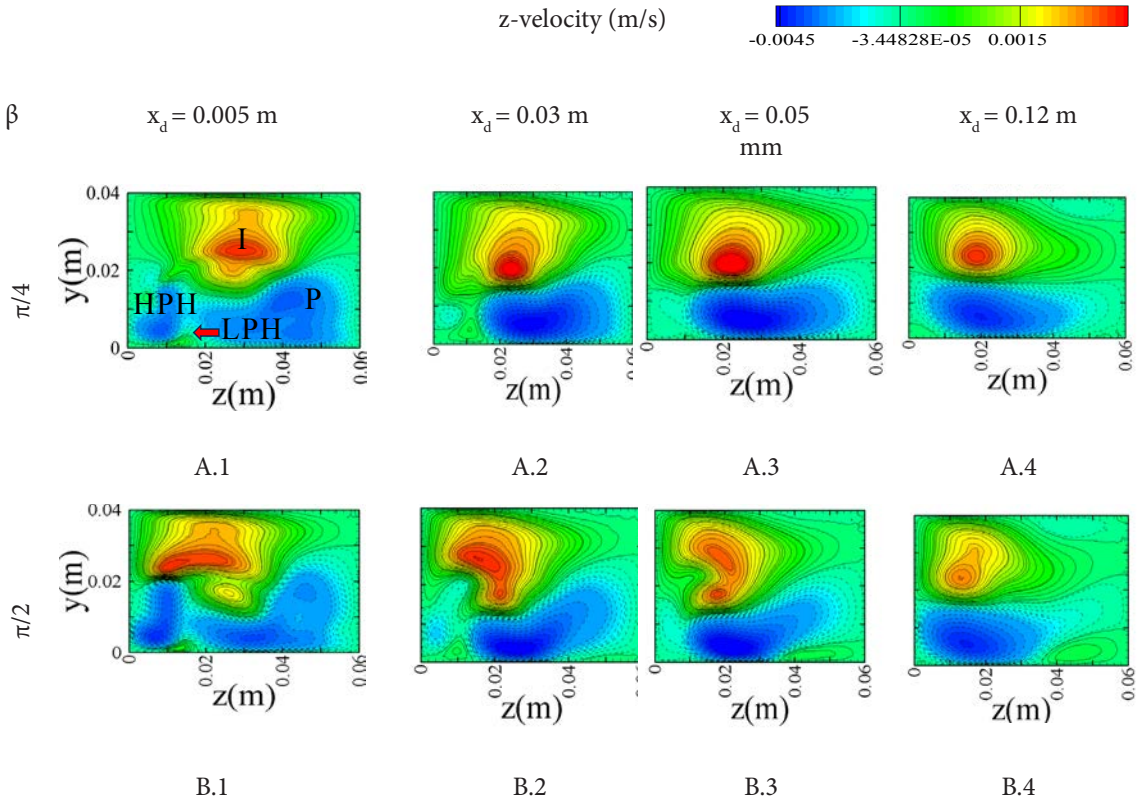

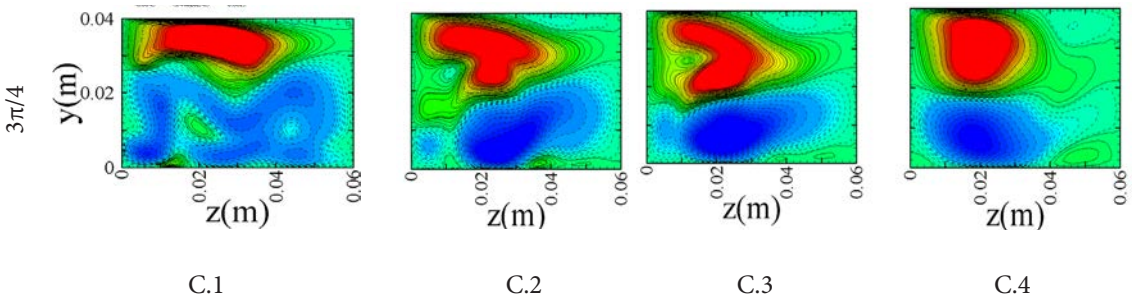

Figure 20. Distribution of z-velocity at different sectional planes downstream of the MRVG where $0 < \beta < \pi$

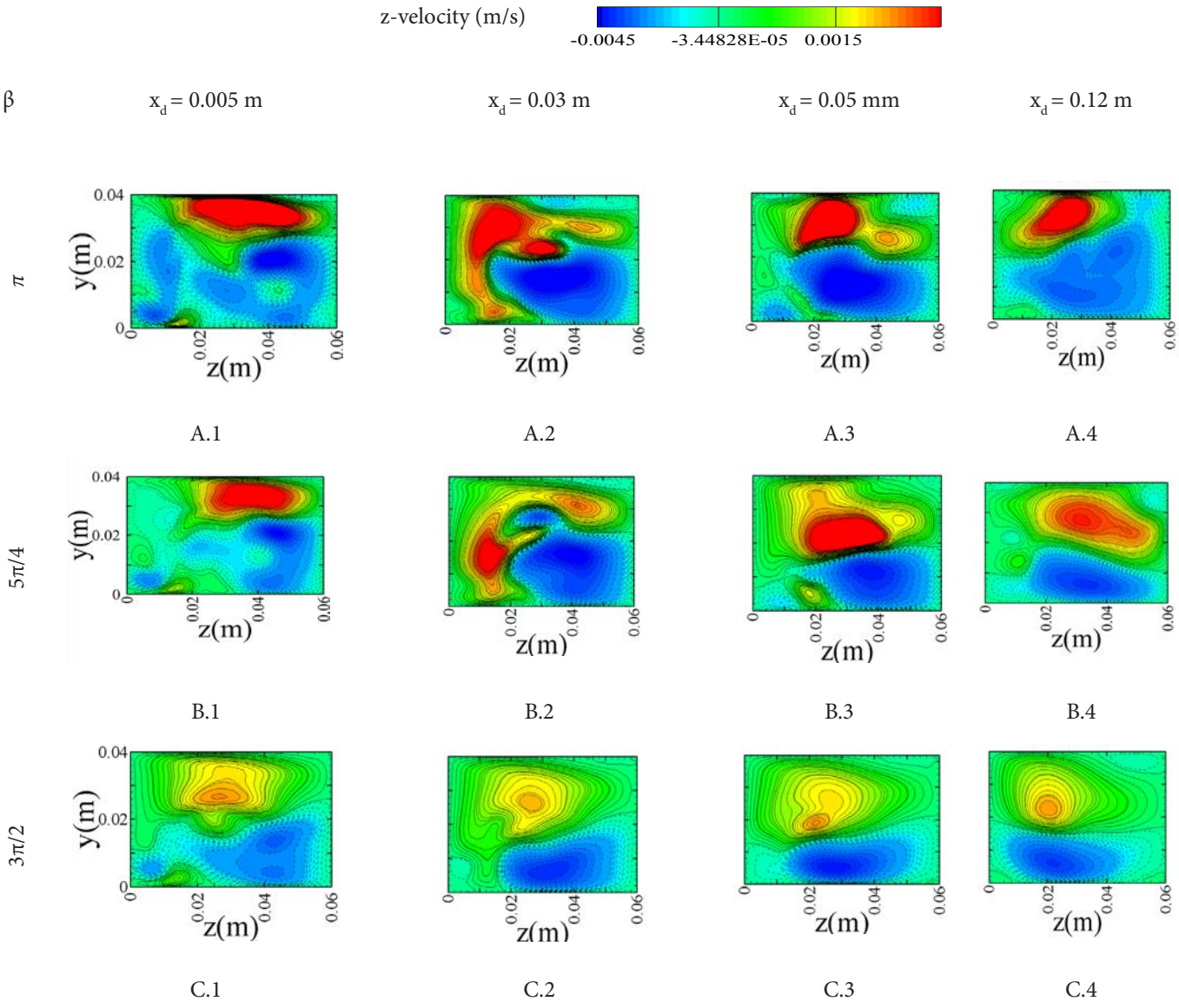

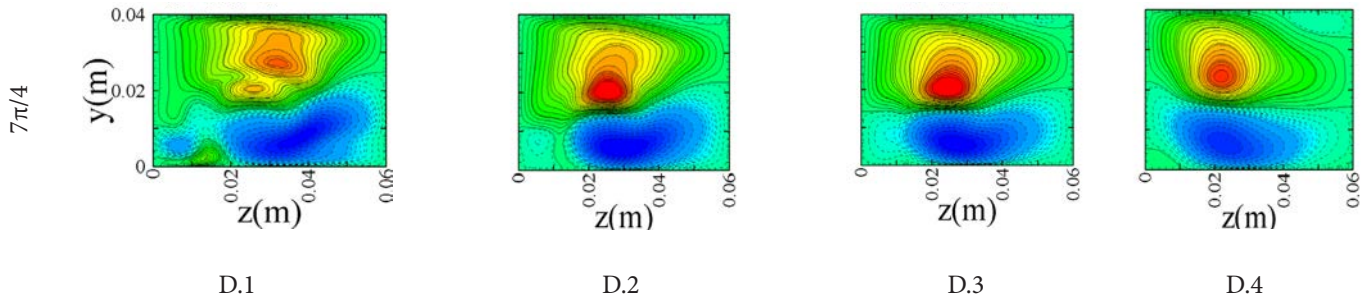

Figure 21. Distribution of z-velocity at different sectional planes downstream of the MRVG where $\pi \leq \beta < 2\pi$

3.3.4.3. Thermal analysis

The main motive for using a VG in a thermal system is to introduce perturbation inside the thermal boundary layer. This perturbation will try to replace the high temperature fluid near the heated plate with low temperature fluid in the free stream. From the various studies in the previous section, it has been observed that the vortices P and I remain alive downstream of the flow for a longer distance. The P in the considered system interacts with the heated bottom plate and remains responsible for dissipation of thermal energy. Figure 22a-g shows the variation in the temperature distribution in a flow section located 0.12 m downstream of the VG. It has been observed that for $\beta = 3\pi/4$ and $\pi/2$, the free stream fluid reaches closest to the bottom plate, replacing the heated fluid in its vicinity. It helps in reducing the thickness of the thermal boundary layer. This increases the temperature gradient between the heated plate and the fluid, and hence, an improvement in heat transfer rate is obtained compared to the other variations of β.

3.3.4.4. Variation of η

Figure 23 shows the η variation with different values of β. It has been observed that the case with $\beta = \pi/2$ yields the highest η, with a 22.4% enhancement compared to the RVG. Owing to the increased value of C_f", the MRVG with $\beta = 3\pi/4$ yields a 19.9% improvement in η. Due to either reduced Nu" or increased C_f" or both, all other cases show a close value of η to that of an RVG.

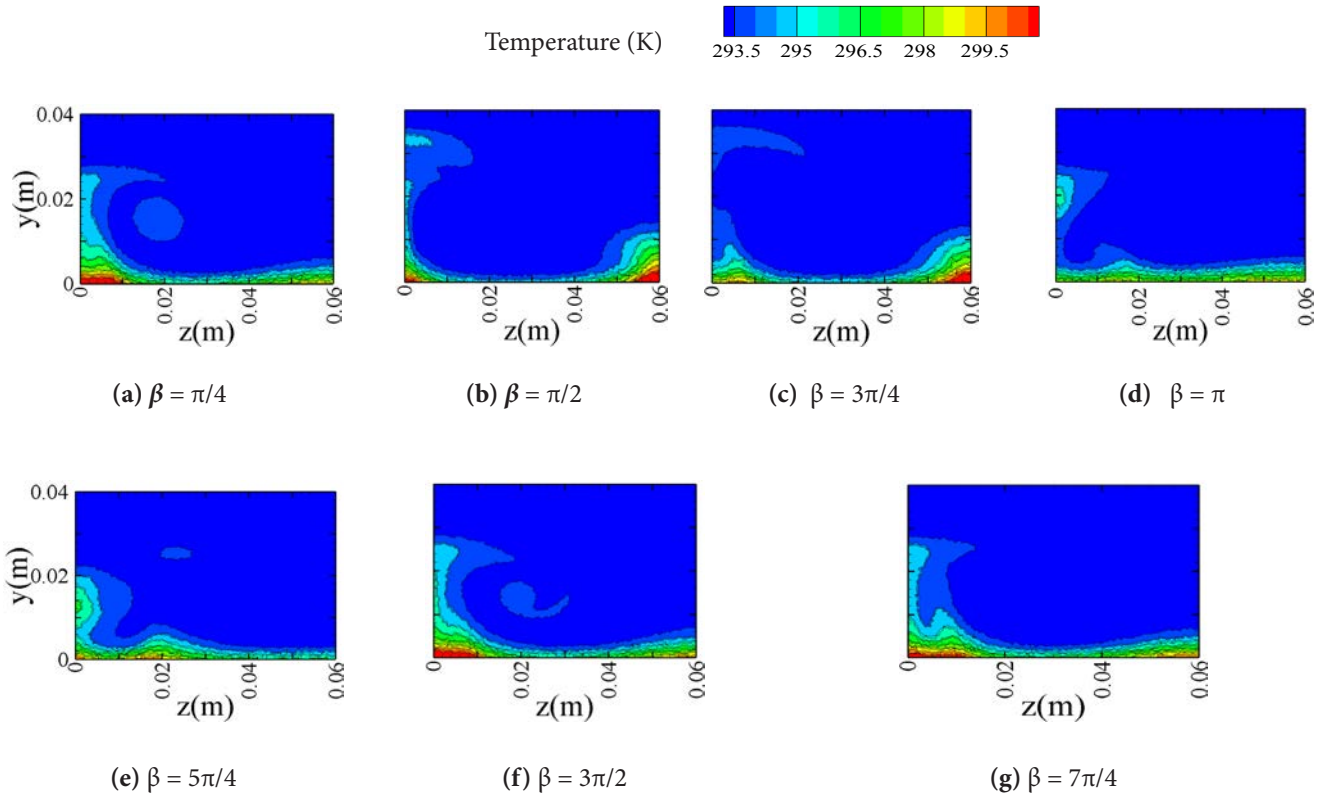

Figure 22. Temperature contours at downstream of the MRVG where $0 < \beta < 2\pi$

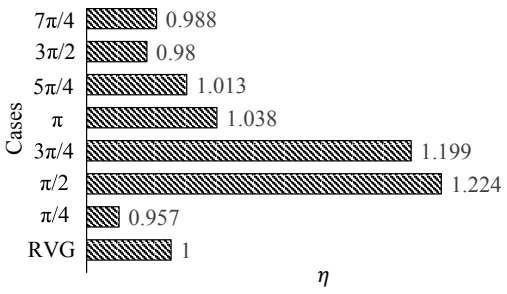

Figure 23. Comparison of η of RVG and different MRVGs with varying β

4. Conclusions

The presence of a modified VG can significantly affect heat transfer from the surface to a cooling fluid. This work evaluates the effect of geometric modifications of the AP of an RVG, on the thermo-hydraulic performance of the system. The work is carried out numerically. The impact of various geometrical parameters of the VG on the flow and the thermal field is analyzed. The governing equations are solved using an FVM solver, which is validated using the numerical results of Abdollahi and Shams [50]. A grid independent solution from the current solver shows good agreement with existing previous published work by Abdollahi and Shams [50], with a maximum deviation of 3.5%. The study provides a detailed analysis of the structure of the formed vortices and the temperature distributions, due to changes in the VG geometry. The findings have practical implications in various engineering applications. Following are the observations taken from the study:

- The interior angles α_1 and α_2 have significant impact on heat transfer. The most significant enhancement occurs when α_1 (= α_2) equals 2π/3, resulting in an 11.13% increase in Nu" compared to the conventional RVG. The maximum values of C_f" and C_d" are observed, when α_1 (= α_2) is 5π/6. However, η reaches its maximum value, when $\alpha_1 = \alpha_2 = 2\pi/3$. At this condition, the maximum increase is 9.9%.
- When $\alpha_1 = \alpha_2 = 2\pi/3$, the width is increased from $0.1h_p$ to $0.5h_p$. As a result, Nu" increases by 27.16%, as compared to the RVG. This enhancement is due to the improved vortex dynamics of the HP and the I.
- The maximum value of h" is 237.27 W/m²K, when $w = 0.5h_p$ and $\alpha_1 = \alpha_2 = 2\pi/3$. In this case, C_f" and C_d" also increase by 11.98% and 14.12%, respectively. It also yields a maximum η of 1.224 compared to the RVG.
- An AP closer to the base plate degrades the thermal performance, while positioning it in line with the top surface of the PP improves C_f" by 11.98%. The obtained value of h" for the configuration is 237.27 W/m^{2}K.
- The Nu" decreases and C_f" and C_d" increase with increasing h_a. The improvement in η of 22.4% is achieved with an MRVG having $\alpha_1 = \alpha_2 = 2\pi/3$, $w = 0.5h_p$, and $h_a = 0.935h_p$.
- The β of the MRVG does not necessarily provide improvement in heat transfer rate. The strength of the vortices reaches its maximum at $\beta = \pi/2$, for $0 < \beta < \pi$. However, as β increases from π to 7π/4, the strength of the vortices gradually reduces. It results in a reduction in the overall heat transfer rate.
- Compared to the RVG, the MRVG with $\beta = 3\pi/4$ shows the maximum increase in Nu" by 27.64%. It also shows a 20.58% increase in C_f". The maximum value of h" is found to be 238.17 W/m^{2}K where $\beta = 3\pi/4$. However, the MRVG configuration with $\alpha_1 = \alpha_2 = 2\pi/3$, $w = 0.5h_p$, $h_a = 0.935h_p$, and $\beta = \pi/2$ achieves an overall heat transfer enhancement (η) of 22.4%.

With the detailed investigation of the considered cases, it has been found that an MRVG with an AP configured with $\alpha_1=\alpha_2 = 2\pi/3$, $w=0.5h_p$, $h_a=0.935h_p$ and $\beta= 3\pi/4$ yields the highest enhancement in Nu" with 27.64%. However, compared to an RVG, the case with $\alpha_1=\alpha_2 = 2\pi/3$, $w=0.5h_p$, $h_a=0.935h_p$ and $\beta= \pi$, yields maximum rise in C_f" and C_d" by 28.88% and 173.85%. Overall, a conjugate heat transfer system demands a balance of enhancement in heat transfer rate with minimum flow losses in the system. In the current study, the MRVG configuration with $\alpha_1=\alpha_2 = 2\pi/3$, $w=0.5h_p$, $h_a=0.935h_p$ and $\beta= \pi/2$, provides the highest increment in thermal performance factor by 22.4%, as compared to RVG. The value of h" for the RVG is 186.59 W/m^{2}K. Under the current configuration, the value of h" for the MRVG is found to be 237.27 W/m^{2}K.

The present work has paved the way for improving the thermal and flow performance of a system with MRVG that utilizes a trapezoid AP. The number of considered cases are limited by considering $\alpha_1=\alpha_2$. Moreover, the common surface of AP and PP is always placed parallel to the bottom plate. Consideration of different angles, α_1, α_2, and the inclination angle of the shared face of AP and PP and its analysis are included as a part of the future endeavor.

Originality statement

The authors declare that this manuscript is original and has not been published or submitted elsewhere.

Authorship contributions

The authors contributed equally to this work.

Funding and/or conflicts of interests/competing interests

The authors have not received funding from any agencies and declare no conflict of interest.

Nomenclature

A_v	frontal projected area of the vortex generator, m^2
c_p	specific heat at constant pressure, J/kg·K
C_d	coefficient of drag
C_d"	surface average coefficient of drag
C_f	skin friction coefficient
C_f"	surface average skin friction coefficient
D_h	hydraulic diameter, m
f	friction factor
F_d	force acting on the frontal projected area, N
h"	surface average heat transfer coefficient, $W/m^2 \cdot K$
h_a	height of auxiliary part, m
h_p	height of principal part, m
k	thermal conductivity of fluid, W/m·K
l_a	length of auxiliary part, m
l_p	length of principal part, m
L_x	length of computational domain, m
L_y	height of the computational domain, m
L_z	width of computational domain, m
Nu	Nusselt number
Nu"	surface average Nusselt number
$\|\vec{q}_y\|$	heat flow rate per unit area (W/m^2)
Ra	Rayleigh number
Re	Reynolds number
t_a	thickness of auxiliary part, m
t_p	thickness of principal part, m
T	temperature, K
T_a	average fluid temperature, K
T_p	average temperature of the heated plate, K
$\vec{v}$	velocity vector, m/s
w	width of auxiliary part, m
x_d	downstream of the vortex generator, m
x_u	upstream of the vortex generator, m

Greek symbols

α_1, α_2	interior angles of APs, rad
β	angle of inclination of AP with PP, rad
η	thermal performance factor
m	dynamic viscosity, N.s/ m^2
n	kinematic viscosity, m^2/s
ρ	density, kg/m3
τ_w	shear stress, N/m^2
φ	angle of attack of the flow, degree

Abbreviations

ACW	anticlockwise
AP	auxiliary part
CDWVG	curved delta winglet vortex generator
COVG	conical offset vortex generator
CTW	curved trapezoidal winglet
CW	clockwise
FVM	finite volume method
HPH	high pressure side horse-shoe vortex
I	induced vortex
LPH	low pressure side horse-shoe vortex
LVG	longitudinal vortex generator
MRVG	modified rectangular vortex generator
P	primary vortex
PP	principal part
RVG	rectangular vortex generator
RWP	rectangular winglet pair
RWVG	rectangular winglet vortex generator
VG	vortex generator
Subscripts	
in	inlet
out	outlet

References

[1] V. Patankar and C. Prakash, "An analysis of the effect of plate thickness on laminar flow and heat transfer in interrupted-plate passages," International Journal of Heat and Mass Transfer, vol. 24, no. 11, pp. 1801–1810, 1981. https://doi.org/10.1016/0017-9310(81)90146-0.

[2] Ramanathan, M. R. Thansekhar, P. R. Kanna, and P. Gunnasegaran, "A new method of acquiring perquisites of recirculation and vortex flow in sudden expansion solar water collector using vortex generator to augment heat transfer," International Journal of Thermal Sciences, vol. 153, pp. 106346, 2020. https://doi.org/10.1016/j.ijthermalsci.2020.106346.

[3] G. Park, "Heat transfer enhancement by a wall-mounted flexible vortex generator with an inclination angle," International Journal of Heat and Mass Transfer, vol. 148, pp. 119053, 2020. https://doi.org/10.1016/j.ijheatmasstransfer.2019.119053.

[4] Sun, K. Zhang, W. Li, Q. Chen, and N. Zheng, "Investigations of the turbulent thermal-hydraulic performance in circular heat exchanger tubes with multiple rectangular winglet vortex generators," Applied Thermal Engineering, vol. 168, pp. 114838, 2020. https://doi.org/10.1016/j.applthermaleng.2019.114838.

[5] Samadifar and D. Toghraie, "Numerical simulation of heat transfer enhancement in a plate-fin heat exchanger using a new type of vortex generators," Applied Thermal Engineering, vol. 133, pp. 671–681, 2018. https://doi.org/10.1016/j.applthermaleng.2018.01.062.

[6] Qian, Q. Wang, and J. Cheng, "Analysis of heat and resistance performance of plate fin-and-tube heat exchanger with rectangle-winglet vortex generator," International Journal of Heat and Mass Transfer, vol. 124, pp. 1198–1211, 2018. https://doi.org/10.1016/j.ijheatmasstransfer.2018.04.037.

[7] Biswas and H. Chattopadhyay, "Heat transfer in a channel with built-in wing-type vortex generators," International Journal of Heat and Mass Transfer, vol. 35, no. 4, pp. 803–814, 1992. https://doi.org/10.1016/0017-9310(92)90248-Q.

[8] Luo, S. Wu, K. Song, L. Hua, and L. Wang, "Thermo-hydraulic performance optimization of wavy fin heat exchanger by combining delta winglet vortex generators," Applied Thermal Engineering, vol. 163, pp. 114343, 2019. https://doi.org/10.1016/j.applthermaleng.2019.114343.

[9] K. Sarangi and D. P. Mishra, "Effect of winglet location on heat transfer of a fin-and-tube heat exchanger," Applied Thermal Engineering, vol. 116, pp. 528–540, 2017. https://doi.org/10.1016/j.applthermaleng.2017.01.106.

[10] J. Modi and M. K. Rathod, "Comparative study of heat transfer enhancement and pressure drop for fin-and-circular tube compact heat exchangers with sinusoidal wavy and elliptical curved rectangular winglet vortex generator," International Journal of Heat and Mass Transfer, vol. 141, pp. 310–326, 2019. https://doi.org/10.1016/j.ijheatmasstransfer.2019.06.088.

[11] Fiebig, A. Valencia, and N. K. Mitra, "Wing-type vortex generators for fin-and-tube heat exchangers," Experimental Thermal and Fluid Science, vol. 7, no. 4, pp. 287–295, 1993. https://doi.org/10.1016/0894-1777(93)90052-K.

[12] A. Gholami, M. A. Wahid, and H. A. Mohammed, "Heat transfer enhancement and pressure drop for fin-and-tube compact heat exchangers with wavy rectangular winglet-type vortex generators," International Communications in Heat and Mass Transfer, vol. 54, pp. 132–140, 2014. https://doi.org/10.1016/j.icheatmasstransfer.2014.02.016.

[13] Sharma, G. Bhushan, and G. Sachdeva, "Effect of flow structure on heat transfer in compact heat exchanger by using finite thickness winglet at acute angle," Journal of Thermal Engineering, vol. 3, no. 2, pp. 1149–1162, 2017. https://doi.org/10.18186/thermal.298616.

[14] GONUL and A. OKBAZ, "Enhanced performance of a microchannel with rectangular vortex generators," Journal of Thermal Engineering, vol. 9, no. 2, pp. 260–278, 2023. https://dx.doi.org/10.18186/thermal.1272395.

[15] Välikangas, S. Singh, K. Sørensen, and T. Condra, "Fin-and-tube heat exchanger enhancement with a combined herringbone and vortex generator design," International Journal of Heat and Mass Transfer, vol. 118, pp. 602–616, 2018. https://doi.org/10.1016/j.ijheatmasstransfer.2017.11.006.

[16] Sun, H. Fu, H. Ma, T. Sun, Y. Luan, and P. Zunino, "Heat transfer enhancement mechanism of elliptical cylinder for minichannels with delta winglet longitudinal vortex generators," International Journal of Thermal Sciences, vol. 198, pp. 108839, 2024. https://doi.org/10.1016/j.ijthermalsci.2023.108839.

[17] Feng, P. Jiang, S. Zheng, Q. Zhang, Z. Chen, F. Guo, and J. Zhang, "Experimental and numerical investigations on the effects of insertion-type longitudinal vortex generators on flow and heat transfer characteristics in square minichannels," Energy, vol. 278, pp. 127855, 2023. https://doi.org/10.1016/j.energy.2023.127855.

[18] Fu, H. Sun, L. Yang, L. Yan, Y. Luan, and F. Magagnato, "Effects of the configuration of the delta winglet longitudinal vortex generators and channel height on flow and heat transfer in minichannels," Applied Thermal Engineering, vol. 227, pp. 120401, 2023. https://doi.org/10.1016/j.applthermaleng.2023.120401.

[19] Liu, J. Teng, J. Chu, Y. Chiu, S. Huang, S. Jin, T. Dang, R. Greif, and H. Pan, "Experimental investigations on liquid flow and heat transfer in rectangular microchannel with longitudinal vortex generators," International Journal of Heat and Mass Transfer, vol. 54, no. 13–14, pp. 3069–3080, 2011. https://doi.org/10.1016/j.ijheatmasstransfer.2011.02.030.

[20] Wang, P. Liu, F. Shan, Z. Liu, and W. Liu, "Effect of longitudinal vortex generator on the heat transfer enhancement of a circular tube," Applied Thermal Engineering, vol. 148, pp. 1018–1028, 2019. https://doi.org/10.1016/j.applthermaleng.2018.11.080.

[21] Ebrahimi, E. Roohi, and S. Kheradmand, "Numerical study of liquid flow and heat transfer in rectangular microchannel with longitudinal vortex generators," Applied Thermal Engineering, vol. 78, pp. 576–583, 2015. https://doi.org/10.1016/j.applthermaleng.2014.12.006.

[22] Zhou and Z. Feng, "Experimental investigations of heat transfer enhancement by plane and curved winglet type vortex generators with punched holes," International Journal of Thermal Sciences, vol. 78, pp. 26–35, 2014. https://doi.org/10.1016/j.ijthermalsci.2013.11.010.

[23] J. Al-Dulaimi, F. A. Kareem, and F. A. Hamad, "Numerical investigation of the heat transfer enhancement inside a square duct with rectangular vortex generators," Journal of Thermal Engineering, vol. 8, no. 1, pp. 1–13, 2022. https://doi.org/10.18186/thermal.1066981.

[24] V. Mundhe and R. S. Bindu, "Numerical and experimental investigations on performance evaluation of a conical offset vortex generator inserts to improve convective heat transfer coefficient," Journal of Thermal Engineering, vol. 6, no. 5, pp. 858–872, 2020. https://doi.org/10.18186/thermal.800276.

[25] Zhou and Q. Ye, "Experimental investigations of thermal and flow characteristics of curved trapezoidal winglet type vortex generators," Applied Thermal Engineering, vol. 37, pp. 241–248, 2012. https://doi.org/10.1016/j.applthermaleng.2011.11.024.

[26] C. Gentry and A. M. Jacobi, "Heat transfer enhancement by delta-wing vortex generators on a flat plate: Vortex interactions with the boundary layer," Experimental Thermal and Fluid Science, vol. 14, no. 3, pp. 231–242, 1997. https://doi.org/10.1016/S0894-1777(96)00067-2.

[27] Xu, M. D. Islam, and N. Kharoua, "Experimental study of thermal performance and flow behaviour with winglet vortex generators in a circular tube," Applied Thermal Engineering, vol. 135, pp. 257–268, 2018. https://doi.org/10.1016/j.applthermaleng.2018.01.112.

[28] Salhi, M. Si-Ameur, and D. Haddad, "Numerical study of natural convection heat transfer performance in an inclined cavity with complex-wavy-wall: nanofluid and random temperature," Computational Thermal Sciences: An International Journal, vol. 7, no. 1, pp. 51–64, 2015. https://doi.org/10.1615/ComputThermalScien.2015013084.

[29] Chafai, H. Salhi, K. Benobouguerra, and S. Chafaa, "Numerical Study of Natural Convection of Nanofluids in an Inclined Flat Bottom Flask Using Finite-Volume Approach," Iranian Journal of Chemistry and Chemical Engineering, vol. 41, no. 7, pp. 2454–2467, 2022. https://doi.org/10.30492/ijcce.2021.527841.4668.

[30] Baiti, H. Salhi, and N. Chafai, "Numerical investigation of turbulent mixed convection in a round bottom flask using a hybrid nanofluid," Advances in Mechanical Engineering, vol. 15, no. 9, pp. 1–12, 2023. https://doi.org/10.1177/16878132231195022.

[31] Salhi and N. Chafai, "Numerical simulation of heat transfer in a square cavity filled with hybrid nanofluid," Nanoscience and Technology: An International Journal, vol. 15, no. 2, pp. 79–94, 2024. https://doi.org/10.1615/NanoSciTechnolIntJ.2023049212.

[32] Zhao, L. Luo, D. Qiu, Z. Wang, and B. Sunden, "On the solar air heater thermal enhancement and flow topology using differently shaped ribs combined with delta-winglet vortex generators," Energy, vol. 224, pp. 119944, 2021. https://doi.org/10.1016/j.energy.2021.119944.

[33] J. Bezbaruah, R. S. Das, and B. K. Sarkar, "Experimental and numerical analysis of solar air heater accoutered with modified conical vortex generators in a staggered fashion," Renewable Energy, vol. 180, pp. 109–131, 2021. https://doi.org/10.1016/j.renene.2021.08.046.

[34] Kumar and A. Layek, "Nusselt number and friction characteristics of a solar air heater that has a winglet type vortex generator in the absorber surface," Experimental Thermal and Fluid Science, vol. 119, pp. 110204, 2020. https://doi.org/10.1016/j.expthermflusci.2020.110204.

[35] J. Bezbaruah, R. S. Das, and B. K. Sarkar, "Overall performance analysis and GRA optimization of solar air heater with truncated half conical vortex generators," Solar Energy, vol. 196, pp. 637–652, 2020. https://doi.org/10.1016/j.solener.2019.12.057.

[36] A. Alnakeeb, M. A. Hassan, and M. A. Teamah, "Thermal performance analysis of corrugated plate solar air heater integrated with vortex generator," Alexandria Engineering Journal, vol. 97, pp. 241–255, 2024. https://doi.org/10.1016/j.aej.2024.04.019.

[37] Hu, Y. Zhang, S. Xie, and Y. Xiao, "Thermo-hydraulic performance of solar air heater with built-in one-eighth sphere vortex generators," Applied Thermal Engineering, vol. 245, pp. 122837, 2024. https://doi.org/10.1016/j.applthermaleng.2024.122837.

[38] S. Sawhney, R. Maithani, and S. Chamoli, "Experimental investigation of heat transfer and friction factor characteristics of solar air heater using wavy delta winglets," Applied Thermal Engineering, vol. 117, pp. 740–751, 2017. https://doi.org/10.1016/j.applthermaleng.2017.01.113.

[39] Tian, Y. Zhang, X. Xiong, G. Gou, and Y. Wu, "Performance enhancement of high temperature fin-and-tube heat exchanger employing winglet combined vortex generators," Applied Thermal Engineering, vol. 249, pp. 123376, 2024. https://doi.org/10.1016/j.applthermaleng.2024.123376.

[40] K. Fahad, N. F. Ifraj, S. H. Tahsin, and M. J. Hasan, "Numerical investigation of the hydrothermal performance of novel vortex generators in a rectangular channel by employing inclination and rotational angles," International Journal of Thermofluids, vol. 20, pp. 100500, 2023. https://doi.org/10.1016/j.ijft.2023.100500.

[41] B. Pérez, A. M. Pérez, and D. S. Suárez, "Influence of the punched holes on thermohydraulic performance and flow pattern of rectangular channels with a pair of perforated vortex generators," International Journal of Heat and Mass Transfer, vol. 184, pp. 122291, 2022. https://doi.org/10.1016/j.ijheatmasstransfer.2021.122291.

[42] J. Modi, N. A. Kalel, and M. K. Rathod, "Thermal performance augmentation of fin-and-tube heat exchanger using rectangular winglet vortex generators having circular punched holes," International Journal of Heat and Mass Transfer, vol. 158, pp. 119724, 2020. https://doi.org/10.1016/j.ijheatmasstransfer.2020.119724.

[43] Caliskan, S. Sevik, and O. Ozdilli, "Heat transfer enhancement by a sinusoidal wavy plate having punched triangular vortex generators," International Journal of Thermal Sciences, vol. 181, pp. 107769, 2022. https://doi.org/10.1016/j.ijthermalsci.2022.107769.

[44] Promvonge, P. Promthaisong, and S. Skullong, "Numerical heat transfer in a solar air heater duct with punched delta-winglet vortex generators," Case Studies in Thermal Engineering, vol. 26, pp. 101088, 2021. https://doi.org/10.1016/j.csite.2021.101088.

[45] Saini, A. Dhar, and S. Powar, "Performance enhancement of fin and tube heat exchanger employing curved delta winglet vortex generator with circular punched holes," International Journal of Thermofluids, vol. 20, pp. 100452, 2023. https://doi.org/10.1016/j.ijft.2023.100452.

[46] Kashyap, K. Das, and B. K. Debnath, "Effect of surface modification of a rectangular vortex generator on heat transfer rate from a surface to fluid," International Journal of Thermal Sciences, vol. 127, pp. 61–78, 2018. https://doi.org/10.1016/j.ijthermalsci.2018.01.004.

[47] Kashyap, K. Das, and B. K. Debnath, "Effect of surface modification of a rectangular vortex generator on heat transfer rate from a surface to fluid: An extended study," International Journal of Thermal Sciences, vol. 134, pp. 269–281, 2018. https://doi.org/10.1016/j.ijthermalsci.2018.08.020.

[48] Kashyap, K. Das, B. K. Debnath, U. Kashyap, and S. K. Saha, "Numerical Study on Effect of Secondary Surface on Rectangular Vortex Generator," Journal of Thermal Science and Engineering Applications, vol. 13, no. 1, pp. 011005, 2021. https://doi.org/10.1115/1.4047008.

[49] P. Incropera, D. P. DeWitt, T. L. Bergman, and A. S. Lavine, Fundamentals of Heat and Mass Transfer, 6th ed. Hoboken, NJ, USA: John Wiley & Sons, 2007.

[50] Abdollahi and M. Shams, "Optimization of heat transfer enhancement of nanofluid in a channel with winglet vortex generator," Applied Thermal Engineering, vol. 91, pp. 1116–1126, 2015. https://doi.org/10.1016/j.applthermaleng.2015.08.066.

List of figure captions